Journal of Neuroinflammation

RESEARCH Open Access

SIRT6 modulates lesion microenvironment in LPC induced demyelination by targeting astrocytic CHI3L1

Jingyi Du[1†], Yue Yin[1†], Dong Wu[1], Can Diao[2], Tiantian Zhao[1], Fan Peng[1], Naigang Li[1], Dongshuang Wang[1], Jiaming Shi[1], Liyan Wang[2], Liang Kong[3], Wenjuan Zhou[1*] and Aijun Hao[1*]

Abstract

Demyelination occurs widely in the central nervous system (CNS) neurodegenerative diseases, especially the multiple sclerosis (MS), which with a complex and inflammatory lesion microenvironment inhibiting remyelination. Sirtuin6 (SIRT6), a histone/protein deacetylase is of interest for its promising effect in transcriptional regulation, cell cycling, inflammation, metabolism and longevity. Here we show that SIRT6 participates in the remyelination process in mice subjected to LPC-induced demyelination. Using pharmacological SIRT6 inhibitor or activator, we found that SIRT6 modulated LPC-induced damage in motor or cognitive function. Inhibition of SIRT6 impaired myelin regeneration, exacerbated neurological deficits, and decreased oligodendrocyte precursor cells (OPCs) proliferation and differentiation, whereas activation of SIRT6 reversed behavioral performance in mice, demonstrating a beneficial effect of SIRT6. Importantly, based on RNA sequencing analysis of the corpus callosum tissues, it was further revealed that SIRT6 took charge in regulation of glial activation during remyelination, and significant alterations in CHI3L1 were obtained, a glycoprotein specifically secreted by astrocytes. Impaired proliferation and differentiation of OPCs could be induced in vitro using supernatants from reactive astrocyte, especially when SIRT6 was inhibited. Mechanistically, SIRT6 regulates the secretion of CHI3L1 from reactive astrocytes by histone-H3-lysine-9 acetylation (H3K9Ac). Adeno-associated virus-overexpression of SIRT6 (AAV-SIRT6-OE) in astrocytes improved remyelination and functional recovery after LPC-induced demyelination, whereas together with AAV-CHI3L1-OE inhibits this therapeutic effect. Collectively, our data elucidate the role of SIRT6 in remyelination and further reveal astrocytic SIRT6/CHI3L1 as the key regulator for improving the remyelination environment, which may be a potential target for MS therapy.

Keywords Remyelination, SIRT6, CHI3L1, Astrocyte, Multiple sclerosis

† Jingyi Du and Yue Yin contributed equally to this work.

*Correspondence:
Wenjuan Zhou
wenjuanzhou@sdu.edu.cn
Aijun Hao
aijunhao@sdu.edu.cn
[1]Key Laboratory for Experimental Teratology of Ministry of Education, Shandong Key Laboratory of Mental Disorders and Intelligent Control, Department of Anatomy and Histoembryology, School of Basic Medical Sciences, Cheeloo College of Medicine, Shandong University, 44#, Wenhua Xi Road, Jinan, Shandong 250012, China
[2]School of Basic Medical Sciences, Cheeloo College of Medicine, Shandong University, Jinan, Shandong 250012, China
[3]Department of Clinical Laboratory, Affiliated Hospital of Shandong University of Traditional Chinese Medicine, Jinan, Shandong, China

Introduction

Multiple sclerosis (MS) is the most common demyelinating disease affecting young adults, characterized by neuroinflammation, oligodendrocyte death, demyelination, reactive gliosis, and axonal degeneration [1]. Subjects with multiple sclerosis experience the deterioration of neurological function, progressive disability, and reduced quality of life both physically and psychosocially [2]. In MS, remyelination is impaired by extrinsic inhibitory cues in the lesion microenvironment including inflammation and reactive glia, as well as by intrinsic defects in oligodendrocyte lineage cells. Promoting remyelination is the core of MS treatment, whereas currently no definitive cure for MS. The lysolecithin (LPC) model is a well-established animal model of local demyelination and remyelination that can simulate some pathologic features of the focal lesions in MS [3], such as myelin and oligodendrocyte loss, significant inflammation, and glial activation [4]. Hence, we would like to utilize the LPC model to identify key factors, to further improve the complex glial response and decipher remyelination-promoting codes in myelin disease.

Sirtuins (SIRTs) are nicotine adenine dinucleotide (NAD^+)-dependent class III histone deacetylases. As an important member of the SIRTs family, Sirtuin 6 (SIRT6) is mainly located in the nucleus, participating in various biological processes, including transcriptional regulation, cell cycling, inflammation, metabolism and longevity, by mediating particular histone H3 lysine deacetylation modifications (epigenetic regulation and post-translational modification) [5–7]. Recent studies have demonstrated the role of SIRT6 in neurological disorders such as ischemic stroke, neurodegenerative disorders, and depressive-like and anxiety-like behaviors [8–13]. SIRT6 is highly expressed in mammalian brain tissues, with widely distributed in multiple cell types. Neuroinflammation and glial responses are important regulatory ways for SIRT6 to exert protective effects. During ischemic brain injury, SIRT6 inhibits microglia activation and potentiates angiogenesis in mice after MCAO [9, 10]. Data primarily from the Alzheimer's disease (AD) mouse model imply that SIRT6 not only regulates the stabilization and level of post-translational modifications to Tau proteins but also attenuates neuroinflammation through the NLRP3 pathway and ameliorates cognitive dysfunction [11, 12]. Moreover, deficiency of SIRT6 in astrocytes of the medial prefrontal cortex (mPFC) modulates depression-like behavior during chronic unpredictable mild stress (CUMS) [13]. However, the role and mechanism of SIRT6 in the CNS demyelination diseases is still poorly understood. Herein, we investigated the important role of SIRT6 in the complex glial responses during myelin regeneration.

Chitinase-3–like protein 1 (CHI3L1) is a secreted glycoprotein and belongs to glycoside hydrolase 18 family. In the CNS, CHI3L1, primarily synthesized and secreted by reactive astrocytes, has been used as a biomarker for a variety of brain pathological conditions, including neuroinflammation, AD, MS, amyotrophic lateral sclerosis (ALS), gliomas, as well as acute diseases, such as traumatic brain injury (TBI) and ischemic stroke [14–19]. In MS, CSF levels of CHI3L1 have a strong correlation with the MS pathologic course, with a progression-dependent manner, and CHI3L1 has been found to be a signaling molecule that activates microglia [16]. As reported, Alexander disease (AxD) is a type of leukodystrophy, caused by mutations in astrocytic glial fibrillary acidic protein (GFAP) gene, resulting in Rosenthal fibers accumulation in astrocyte, and AxD mice model exhibits astrocyte dysfunction and OPCs/oligodendrocyte loss and myelination defect [20]. In particular, transcriptomic analyses of post-mortem samples from AxD patients and iPSC astrocytes identified CHI3L1 as a key mediator of AxD astrocyte-induced inhibition of OPCs activity [21]. The above studies indicate that astrocytic CHI3L1 is an important pathway in neuronal-glial or astrocytic crosstalk with other cells, and a potential therapeutic target for CNS demyelinating diseases.

In the present study, we investigated the role and potential mechanisms of SIRT6 in LPC induced demyelination. This study has provided some evidence for the mechanisms of astrocytic SIRT6/CHI3L1 following demyelination injury, highlighting its potential utility as the key regulator of remyelination environment in the CNS.

Materials and methods

Animals

Adult female C57BL/6J mice (8–10 weeks old and 20–25 g) were purchased from Beijing Vital River Laboratory Animal Technology (Beijing, China). Mice were housed in SPF environment with a 12 h/12 h light/dark cycle and controlled temperature (22±1 °C). Food and water were supplied ad libitum. All animal care and experiments were approved by the Institutional Animal Care and Use Committees of Shandong University (Accreditation number: SYXK:20230003) and according to National Institutes of Health Guide for the Care and Use of Laboratory Animals.

Stereotaxic surgery and drug administration

Demyelination was induced by LPC injury as previously described with minor modifications [22]. In brief, mice were anesthetized with isoflurane (induced at 3%, and maintained at 1.5%) and then positioned in a stereotaxic frame (68507, RWD, China) with a heating pad to maintain body temperature at 37 °C during surgery.

The mice were injected with 2 μL of 1% LPC (#9008-30-4; Sigma-Aldrich) in sterile saline solution into bilateral corpus callosum with a 5 μL Hamilton syringe (Bregma: AP+1.0 mm; ML±1.0 mm; DV −2.3 mm). The rate of injection was 0.5 μL/min. Mice in Control group were injected with 2 μL saline at each point. After injection, the needle was kept for 10 min and then slowly retracted. On this basis, mice received subsequent injections of drugs or AAV, and mice were subjected to behavioral testing or sacrificed followed by designated experimental schedules in different sections.

OSS_128167, a selective SIRT6 inhibitor (#887686-02-4; MedChemExpress, USA), at concentrations of 20 μg/3μL was bilaterally injected into the ventricle following LPC injection immediately (Bregma: AP+1.0 mm; ML±0.5 mm; DV − 3.0 mm). Mice were divided into four groups: (i) Control, (ii) OSS, (iii) LPC, and (iv) LPC+OSS.

MDL is a selective allosteric SIRT6 deacetylase activator (SML2529; Millipore-Sigma, USA) [23]. After the brain stereotaxic surgery, MDL-800 was administered by daily intraperitoneal injections at a dosage of 10 mg/kg (body weight) for 14 days [24]. Mice were divided into four groups: (i) LPC, (ii) LPC+OSS, (iii) LPC+MDL, and (iv) LPC+OSS+MDL.

Isolation and treatment of primary cells

Primary cultures of astrocytes and OPCs from the mouse cortex were established and maintained as described elsewhere [25, 26]. Briefly, the mix glial cells were dissected from neonatal mice pups (1-day-old) with the aseptic operation after meninges and vessels stripped, and digested with 0.25% trypsin/EDTA (#CC012; Gibco, USA) at 37 °C for 10 min. The cells were cultured in poly-L-lysine-coated T75 flasks (Corning, USA) with Dulbecco's modified Eagle's medium-high-glucose medium (#6124153; DMEM-HG, Gibco, USA) containing 10% fetal bovine serum (FBS, Gibco, USA) and 1% penicillin-streptomycin mixture (#CC033; Gibco, USA). The medium was changed every 3 days. After 8–10 days, mix glial cells were shaken at 200 rpm and 37 °C for 2 h to remove microglia. The remained mixed glia changed fresh DMEM-HG medium. And then the mix glial cells underwent another shake at 220 rpm for 18–20 h in a 5% CO2 incubator at 37 °C, during which astrocytes were attached to the bottom, while OPCs still suspended in the medium. OPCs were collected and seeded onto poly-L-lysine-coated coverslips with DMEM/F12 (#6123063; Gibco, USA) supplemented with 1% N2, 2% B27, 0.1% bovine serum albumin, 10 ng/mL PDGF, 10 ng/mL bFGF and 1% penicillin/streptomycin for 2 days. And 50 ng/mL T3 and 10 ng/mL CNTF were used to induce OPCs differentiation. Astrocytes were cultured at desired densities in 6-well plates.

Cultured astrocytes were treated with 300 μM OSS128_167 [27], 10 μM MDL800 [28] or 0.1‰ DMSO for Vehicle group for 24 h, followed by application of 1 μg/mL lipopolysaccharide (LPS, Sigma-Aldrich, USA) for a further 24 h. Cultured astrocytes were divided into four groups: (i) Control, (ii) LPS, (iii) LPS+OSS, and (iv) LPS+MDL. And astrocytic conditioned media (AST-CM) were collected and centrifuged at 1000 g for 5 min to remove debris and dead cells, and then filtered through the syringe filters (0.22 μm pore size, Millipore, USA). OPCs or differentiated OPCs were incubated with the supernatant mixed with AST-CM at a ratio of 1:2 for 24 h before immunocytochemical staining.

Neurobehavioral assessment

For behavioral tests, the assessors were blinded to the expreimental groups in all outcome measures.

Morris water maze

Morris water maze (MWM) test was performed to evaluate spatial learning and memory ability. The water maze was an opaque circular pool with a diameter of 120 cm and a height of 40 cm, divided into four quadrants and indicated by prominent extra maze cues. An invisible platform (10 cm diameter) was placed 1 cm beneath the surface of the water in target quadrants. MWM contained place navigation training and subsequent spatial probe test. During the acquisition phase, mice were allowed 60 s to find the platform from four different quadrants. The searching time was recorded as latency time. Mice were guided to the platform and stayed for 30 s if failing to find the platform within 60 s, and then the time was recorded as 60 s. On the sixth day for the probe test, the platform was removed. Mice were released from the opposite side of the target quadrant and allowed to explore the maze for 60 s, and the swimming path to reach the platform, the time spent in the target quadrant, and the platform crossing time were recorded using tracking software.

Novel object recognition test

Novel object recognition (NOR) test has been widely used to detect memory function. The test included 3 phases: habituation, training and test. During the habituation phase, mice were allowed to adapt in the apparatus (40 cm × 40 cm × 30 cm) for 10 min. 24 h later, in the training stage, two identical objects were placed in the box, and mice were allowed to explore freely in 10 min. And on the next day, before the test, one familiar object was replaced by a new object with different color and shape. During the test phase, the exploration time for mice was 10 min, and the exploration time spent on new (N) and familiar (F) objects was record by software. Recognition index=N / (N+F) × 100%.

Open field test

To determine spontaneous locomotor activity, Open Field Test (OFT) was carried out. The apparatus was a 40 cm × 40 cm square area with 30 cm-high sidewalls. Mice were placed in the center of the apparatus and allowed to freely explore for 10 min. The video-recording of locomotor activity started immediately after the mouse is placed in the box. Total distance traveled was measured for analysis. Between each experiment, the apparatus was cleaned with 75% ethanol to avoid any interference with subsequent tests.

Rotarod test

To evaluate limb motor coordination and balance of mice, the rotarod test was performed. Before testing, mice underwent 3 days of adaptation training in the rotarod apparatus. For the testing, mice were placed on the accelerating automated rotating rod, which the speed was gradually accelerated from 4 r/min to 40 r/min within 60 s, then maintained the same speed for 300 s. Each mouse was tested 3 times for repeated testing the latency to fall and calculated the average as results.

Luxol fast Blue (LFB) staining

The sacrificed mice were deeply anesthetized and transcardially perfused with 40 ml 0.9% physiological saline, followed by 40 mL 4% paraformaldehyde (PFA). Mouse brains were fixed with 4% PFA at 4 °C for 24 h, and then dehydrated using 20% and 30% sucrose solution until they completely sunk. Successively, brain samples were cut into coronal Sect. (14 μm thick) with a frozen slicer (Thermo, USA) at -20 °C and stored in -80 °C.

LFB histological staining was conducted to evaluate myelin content and integrity at the lesion sites. Briefly, after washed in PBS, brain sections were immersed in LFB solution (#1328-51-4; Solarbio, China) at 60 °C for 6–8 h, then cooled to room temperature and differentiated in 0.05% Li2CO3 (Solarbio, China) and 70% alcohol. The sections were washed in distilled water, and then sequentially dehydrated with graded ethanol, followed by mounted with neutral gum (#96949-21-2; Solarbio, China) and captured by microscope (Olympus, Japan). The area of demyelination in corpus callosum was calculated using Image J. For semi-quantitative analysis, 5 sections per mouse were screened from 3 mice per group.

Immunofluorescence

For immunofluorescence staining, the slices or the OPCs were blocked with 10% (w/v) donkey serum (#SL050; Solarbio, China) and 0.1% Triton X-100 (#9002-93-1; Solarbio, China) in PBS at 37 °C for 2–3 h. And then incubated with primary antibodies at 4 °C overnight (rabbit anti-SIRT6, ab191385, 1:200, Abcam; rabbit anti-MBP, 78896 S, 1:200, CST; rabbit anti-PDGFRα, 3174 S, 1:200, Abcam; rabbit anti-CC1, ab40778, 1:500, Abcam; rabbit anti-Iba1, 019-10741, 1:400, Wako; mouse anti-GFAP, 3670 S, 1:400, CST; rabbit anti-CHI3L1, 12036-1-AP, 1:200, Proteintech; goat anti-OLIG2, AF2418, 1:50, R&D). On the following day, after washing with PBS, sections and cell coverslips were incubated with secondary antibodies at room temperature for 1 h, including Alexa Fluor 594-conjugated antibody (A21207; 1:500, Invitrogen), Alexa Fluor 488-conjugated antibody (A32814; 1:500, Invitrogen), Alexa Fluor 594-conjugated antibody (A21203; 1:500, Invitrogen), Alexa Fluor 488-conjugated antibody (A21202; 1:500, Invitrogen). Nuclei were counterstained with DAPI. Images were acquired using a fluorescence microscope (Olympus, Japan) and measured with Image J software.

Electron microscopy

After the mice were sacrificed, the injection lesion of corpus callosum tissues were cut into the 1 mm*1 mm*1 mm cube and fixed in 2.5% glutaraldehyde at 4 °C overnight. After washing with PBS, the tissues were post-fixed in 2% OsO4 at 4 °C, and then subjected to graded ethanol dehydration series. Finally, the tissues were embedded in epoxy resin. Tissue slicing (50 nm thick) was prepared for Transmission electron microscopy (TEM) observation with an electron microscope (Talos F200C G2, FEI, USA). The number of demyelinated axons and g-ratio was analyzed using the Image J software.

Western blotting

After the mice were sacrificed, the injection lesion of corpus callosum tissues were rapidly sliced and picked out using coronal brain matrices at intervals of 1 mm, immediately frozen in liquid nitrogen and stored at −80 °C until use. Total protein from corpus callosum tissues was extracted using RIPA Buffer (P0013B; Beyotime, China) supplemented with protease inhibitor (Beyotime, China), and the protein concentration of samples was determined using the BCA assay kit (Yeasen, China). Tissue lysates (15 μg) were loaded onto a 10% SDS-polyacrylamide gel. After gel electrophoresis, proteins were transferred onto polyvinylidene fluoride (PVDF) membranes (0.22 μm, Millipore, USA) using the electrophoretic transfer tank (Bio-Rad, USA). The membranes were blocked with 5% nonfat milk and incubated with various primary antibodies at 4 °C overnight. Primary antibodies were used: rabbit anti-MOG, 12690-1-AP, 1:500, Proteintech; rabbit anti-MBP, 78,896 S, 1:1000, CST; rabbit anti-MAG, 14386-1-AP, 1:500, Proteintech; rabbit anti-PDGFRα, 3174 S, 1:1000, Abcam; rabbit anti-CC1, ab40778, 1:500, Abcam; rabbit anti-CNPase, 5664 S, 1:500, CST; mouse anti-SOX10, 66786-1-Ig, 1:1000, Proteintech; mouse anti-β-actin, 66009-1-Ig, 1:500, Proteintech; rabbit anti-acetyl-histone H3 (Lys9) (H3K9ac), 9649 S, 1:500, CST;

rabbit anti-acetyl-histone H3 (Lys56) (H3K56ac), 4243 S, 1:500, CST; rabbit anti-H3, 4499 S, 1:1000, CST; rabbit anti-SIRT6, ab191385, 1:500, Abcam; rabbit anti-CHI3L1, ab319164, 1:500, Abcam. After washing with PBS containing 1% Tween-20, the membranes were then incubated within appropriate HRP-conjugated anti-mouse or anti-rabbit IgG at room temperature for 1 h. Finally, membranes were treated with enhanced ECL detection system (Merck Millipore). Quantification was analyzed using Image J software (Image J 1.53e). Briefly, the density intensity of each band was measured; then, the relative levels of protein were normalized for each well of the β-actin protein levels, and for acetylation it is normalized of H3. The protein / β-actin (or H3) ratios of treated samples were normalized to the control protein / β-actin (or H3) ratios. Each experiment was performed at least three times (or at least three animals).

Real-time quantitative PCR (RT-PCR) analysis

Total RNA from corpus callosum tissues or cultured astrocytes were extracted using Trizol reagent (#10606ES60; Invitrogen), and quantified by Nanodrop 2000. The cDNA was synthesized from 1 μg RNA using cDNA Synthesis Kit (#11141ES60; Yeasen, China), according to the manufacturer's instructions. The PCR assays were performed using the SYBR Green Kit (#11201ES08; Yeasen, China) on CFX Connect Real-Time system (Bio-Rad, USA) under the following conditions: 5 min at 95 °C, 40 cycles at 95 °C for 10 s and 60 °C for 30 s. β-actin was used as an internal control. The primer sequences were as follows: β-actin Forward: CGTTGAC ATCCGTAAAGACCTC, Reverse: CCACCGATCCAC ACAGAGTAC; SIRT6 Forward: TGACACCACCTTC GAGAATGCT, Reverse: AGACAAATCGCTCCACCA AC; OLIG2 Forward: GGGAGGTCATGCCTTACGC, Reverse: CTCCAGCGAGTTGGTGAGC; PDGFRα Forward: TCCATGCTAGACTCAGAAGTCA, Reverse: TC CCGGTGGACACAATTTTTC; CNPase Forward: TTT ACCCGCAAAAGCCACACA, Reverse: CACCGTGTC CTCATCTTGAAG; MBP Forward: GGCGGTGACAGA CTCCAAG, Reverse: GAAGCTCGTCGGACTCTGAG; CHI3L1 Forward: GTACAAGCTGGTCTGCTACTTC, Reverse: ATGTGCTAAGCATGTTGTCGC; C3 Forward: CCAGCTCCCCATTAGCTCTG, Reverse: GCACTTG CCTCTTTAGGAAGTC; S100a10 Forward: TGGAAA CCATGATGCTTACGTT, Reverse: GAAGCCCACTTT GCCATCTC. The data of real-time PCR were analyzed using the value $2^{-\triangle\triangle Ct}$.

Chromatin immunoprecipitation (ChIP) assay

The ChIP assays were performed by SimpleChIP® Enzymatic Chromatin IP Kit (9003 and 9005, CST, USA) according to the manufacturer's protocol. In brief, cultured astrocytes or corpus callosum tissues were collected and fixed with 1% formaldehyde at 37 °C for 10 min. After cells were washed and lysed by nuclease, appropriate genomic DNA fragments were obtained by sonicating cell lysates. To precipitate the chromatin, anti-acetyl-histone H3 (Lys9) (H3K9ac) (9649 S, CST) were incubated overnight at 4 °C, and normal rabbit IgG as negative controls, followed by immunoprecipitation with protein G magnetic beads. After washing, elution, and reversing the cross-links, the DNA was extracted, purified from the binding complex and analyzed by real-time PCR. The primer sequences were as follows: CHI3L1-#1 promoter Forward: GACCCGTCAACCGTCTTC, Reverse ATGGCAGGATGTTTCTCA; CHI3L1-#2 promoter Forward: CAACGGACCGCCTAACAG, Reverse GGTATCTGAGACCCTTGAC. The relative enrichment of promoter DNA was normalized to the input.

In vitro cell transfection

The RNAi for CHI3L1 and negative control were obtained from MiaoLingBio (Wuhan, China). Primary astrocytes were cultured in complete medium in 6-well plates for 48 h, and RNAi were transfected into astrocytes using Lipofectamine 3000 (Invitrogen, USA) according to the manufacturer's protocol for 6–8 h. The mixture was removed and then followed by LPS or LPS+OSS treatment.

Adeno-associated virus-mediated overexpression experiment

Adeno-associated virus (AAV) serotype 9 that delivers Astrocytes-specific GFaABC1D promoter driving murine SIRT6 expression or murine CHI3L1 expression and control viruses only containing GFP protein or RFP protein were produced by Vigene Biosciences (Shandong, China). Mice were randomly divided into four groups: Control, LPC, LPC+AAV-SIRT6OE, LPC+AAV-SIRT6OE+AAV-CHI3L1OE. Lesion areas SIRT6 or CHI3L1 overexpression was achieved by bilaterally stereotaxic injection of AAV-SIRT6OE (1.0×10^{10} vg/mouse) or AAV-CHI3L1OE (1.0×10^{10} vg/mouse) using the following coordinates: Bregma: AP+1.0 mm; ML±1.0 mm; DV −2.3 mm, 5 days before LPC injection at same sites. After 14 days, mice were subjected to behavioral tests or histopathological tests.

RNA-sequencing and analysis

The total RNA of corpus callosum was extracted through Trizol reagent by following the manufacturer's protocol in the Control, LPC, LPC+OSS and LPC+MDL groups. Equal amounts of RNA from three samples were mixed together. RNA-sequencing was performed by BGI Company with the Illumina HiSeq™ 2000 platform (Wuhan, China). The sequencing data were analyzed on the GENEAN Cloud Platform (biosys.bgi.com). Differentially

expressed genes (DEGs) with statistical significance were identified through Scatter Plot filtering. The threshold required for the results to be considered significant was as follows in each comparison group: q value≤0.05 and absolute value of |log2 (Fold Change)| ≥ 1.0. The Kyoto Encyclopedia of Genes and Genomes (KEGG) and Heatmap of the DEGs was implemented with the Bgi multiomics system.

Statistical analysis

All data were analyzed using GraphPad Prism 8.0 (GraphPad Software, USA). For most analyses, one-way analysis of variance (ANOVA) was followed by Tukey's test for multiple comparisons. For some select analyses, unpaired Student's t test was used to compare between two variables. A value of $P<0.05$ was considered to indicate statistical significance.

Results

Expression pattern of SIRT6 in LPC-induced corpus callosum demyelination

To determine whether SIRT6 is associated with LPC-induced injury, we used local demyelination mice model with LPC injection into the CC (Fig. 1A). As shown in Fig. 1B-E, western blotting of myelin associated markers, MOG, MBP and MAG, revealed the de-/remyelination dynamics process in LPC model that we established (Fig. 1C; $F_{3,12} = 27.01$, one-way ANOVA; Fig. 1D; $F_{3,12} = 14.87$, one-way ANOVA; Fig. 1E; $F_{3,12} = 45.95$, one-way ANOVA). Consistent with previous reports, the demyelination occurs in early stage (3 ~ 7 days post injury (dpi)) with the lower expression level of myelin related proteins, and remyelination starts from 10 ~ 14 dpi until 28 dpi. And results of qPCR analysis showed that SIRT6 mRNA levels in the local lesion area increased at 7 dpi, peaked at 14 dpi and decreased to the baseline at 28 dpi (Fig. 1F; $F_{3,12} = 210.0$, one-way ANOVA). Then we examined the immunofluorescence intensity of SIRT6 in CC at 14 dpi. Immunofluorescence assay found that mean intensity of SIRT6 was significantly higher after LPC injury (Fig. 1G, H; $P<0.0001$, two-tailed t-test). We further detected the co-localization of SIRT6 expression with markers of different cell types using immunofluorescence. The results showed that it is expressed in astrocytes, oligodendrocytes and microglia (Fig. 1I). These findings suggested SIRT6 appeared to correlate with demyelinated complex microenvironment and participated in myelination dynamics process.

Inhibition of SIRT6 exacerbated motor and cognitive dysfunction after LPC injury

To determine the role of SIRT6 in remyelination, we performed pharmacological inhibition of SIRT6 by OSS_128167 treatment, a potent selective SIRT6 inhibitor, to suppress the activity of SIRT6. Briefly, mice in LPC+OSS group were subjected to LPC injection into CC, and then OSS_128167 was injected into bilateral lateral ventricles, according to the designated experimental schedules (Fig. 2A). Firstly, the range of applicable concentration of OSS_128167 (3 μg/3μL, 20 μg/3μL, 60 μg/3μL) was examined by qPCR at 14 dpi in demyelinated CC. Among them, 20 μg/3μL was able to significantly reduce the proliferation and differentiation of oligodendrocyte precursor cells (OPCs), with the expression of markers, PDGFRα and CNPase, decreased respectively. And the expression of oligodendrocyte lineage marker, Olig2, was mildly inhibited (Fig. 2B; $F_{3,8} = 206.5$, one-way ANOVA). Meanwhile, no significant change in SIRT6 mRNA levels was found when control mice treated with 20 μg/3μL OSS_128167 (Fig. S1A; $F_{3,8} = 2.14$, $P=0.1732$, one-way ANOVA). Western blotting of protein samples collected 14 days after LPC injury, showed that the acetylation levels of specific histone deacetylation sites (H3K9 and H3K56) for SIRT6 were increased with OSS treatment (Fig. S1B-D, Fig. S1C; F3,12=69.90, one-way ANOVA; Fig. S1D; F3,12=91.40, one-way ANOVA), and the expression levels of SIRT6 protein were suppressed (Fig. S2A-B; F3,8=323.1, one-way ANOVA). Hence, 20 μg/3μL of OSS_128167 was chosen for subsequent experiments. As reported, CC is closely associated with motor and cognitive functions, and damage to white matter myelin in this region leads to corresponding neurological impairment [29–31]. We subsequently investigated whether inhibition of SIRT6 interferes with motor and cognitive functions in LPC mice. The Morris water maze (MWM) and the Novel Object Recognition (NOR) test were conducted to evaluate the OSS_128167 effects on learning and memory after LPC injury. In the MWM test, mice treated with LPC spent significantly more time and longer path length on finding the platform during the acquisition/learning period, and the OSS_128167 aggravated abnormal performance (Fig. 2C, two-way ANOVA). In the probe test, the LPC+OSS group performed significantly worse for the target quadrant, compared to the LPC group ($P=0.0060$) and Control group ($P<0.0001$), and the frequency of crossing over the platform was significantly lower in LPC+OSS group than that of LPC group ($P=0.0135$) and Control group ($P<0.0001$) (Fig. 2D; $F_{3,20} = 43.46$, one-way ANOVA; Fig. 2E; $F_{3,20} = 103.4$, one-way ANOVA). Then, the LPC+OSS mice showed discrimination in NOR test, with the lower novel object preference index, compared to the LPC group ($P=0.0204$) and Control group ($P<0.0001$) (Fig. 2G; $F_{3,20} = 54.16$, one-way ANOVA). Besides, the motor behavior was evaluated by Open Field test (OFT) and Rotarod, which evaluated balance, grip strength, and motor coordination. As shown in Fig. 2H, reduced distance traveled was detected

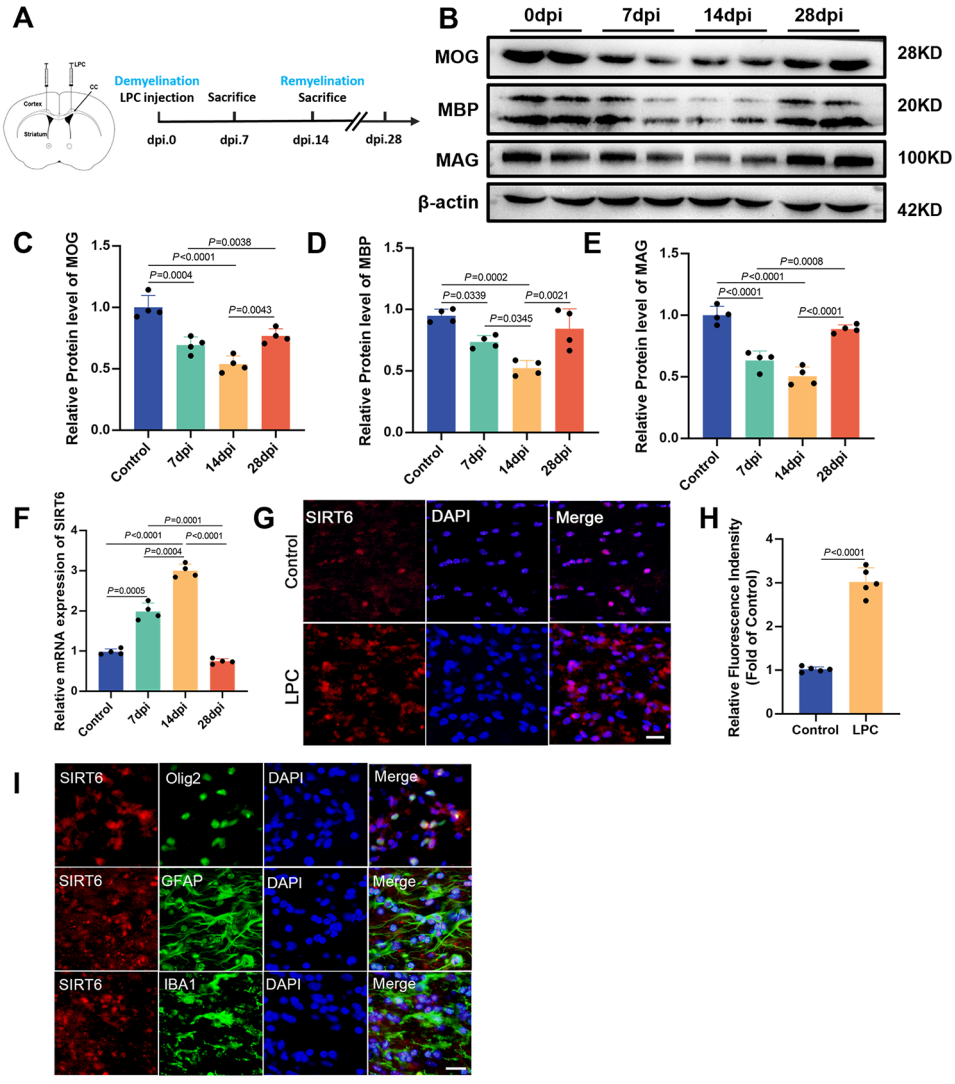

Fig. 1 Changes in SIRT6 in the corpus callosum at 0, 7, 14, 28 days post-last injury in LPC mice **A** Schematic depicting the experimental approach and timeline. Mice were subjected to bilateral LPC injection into CC. At 0, 7, 14, 28 dpi after LPC injection, mouse tissue was collected for histopathological, biochemical analyses. **B** Representative images of western blotting of MOG, MBP, MAG and β-actin at 0, 7, 14, 28 dpi after LPC injection. **C-E** Quantification of protein expressions of MOG (**C**), MBP (**D**), MAG (**E**) (one-way ANOVA with Tukey's multiple-comparison test, $n = 4$ per group). **F** Expressions of mRNA of SIRT6 at 0, 7, 14, 28 dpi after LPC injection (one-way ANOVA with Tukey's multiple-comparison test, $n = 4$ per group). **G** SIRT6 immunofluorescence staining of corpus callosum tissue sections showed a significant increase of SIRT6-positive cells at 14 dpi in LPC mice. Red: SIRT6, Blue: DAPI, scale bar = 25 μm. **H** Quantitative analysis of SIRT6 relative fluorescence intensity (two-tailed unpaired Student's t-test, $n = 5$ per group). **I** Immunostaining of SIRT6 (red) or OLIG2 (green), GFAP (green), IBA1 (green) and DAPI (blue) in CC at 14 dpi after LPC injury, scale bar = 25 μm. Data: $P < 0.05$ is statistically significant. All values are denoted as the mean ± SD

in LPC+OSS group (Fig. 2H; $F_{3,20}$ = 23.04, one-way ANOVA). And OSS_128167 treatment impaired motor function after LPC injury, as suggested by the lower latency to fall from the rotating rod when compared to LPC (P=0.0097) and Control mice (P<0.0001) (Fig. 2I; $F_{3,20}$ = 107.7, one-way ANOVA). As expected, OSS group had no significant effect on the performance of mice in above behavior tests. These results indicated that inhibition of SIRT6 developed more severe cognitive and motor dysfunction after LPC injury.

Remyelination impairments were significantly induced by SIRT6 inhibitor in the demyelinated lesions

To investigate whether inhibition of SIRT6 caused increased myelin damage, we analyzed the morphological structure of white matter myelin. It has been previously reported that OSS_128167 can reduce SIRT6 expression at a later stage [32]. Therefore, we immediately injected SIRT6 inhibitor bilaterally into the ventricle following LPC injection. Luxol Fast Blue (LFB) staining and immunofluorescence were performed to assess severity of myelin injury. LFB results showed

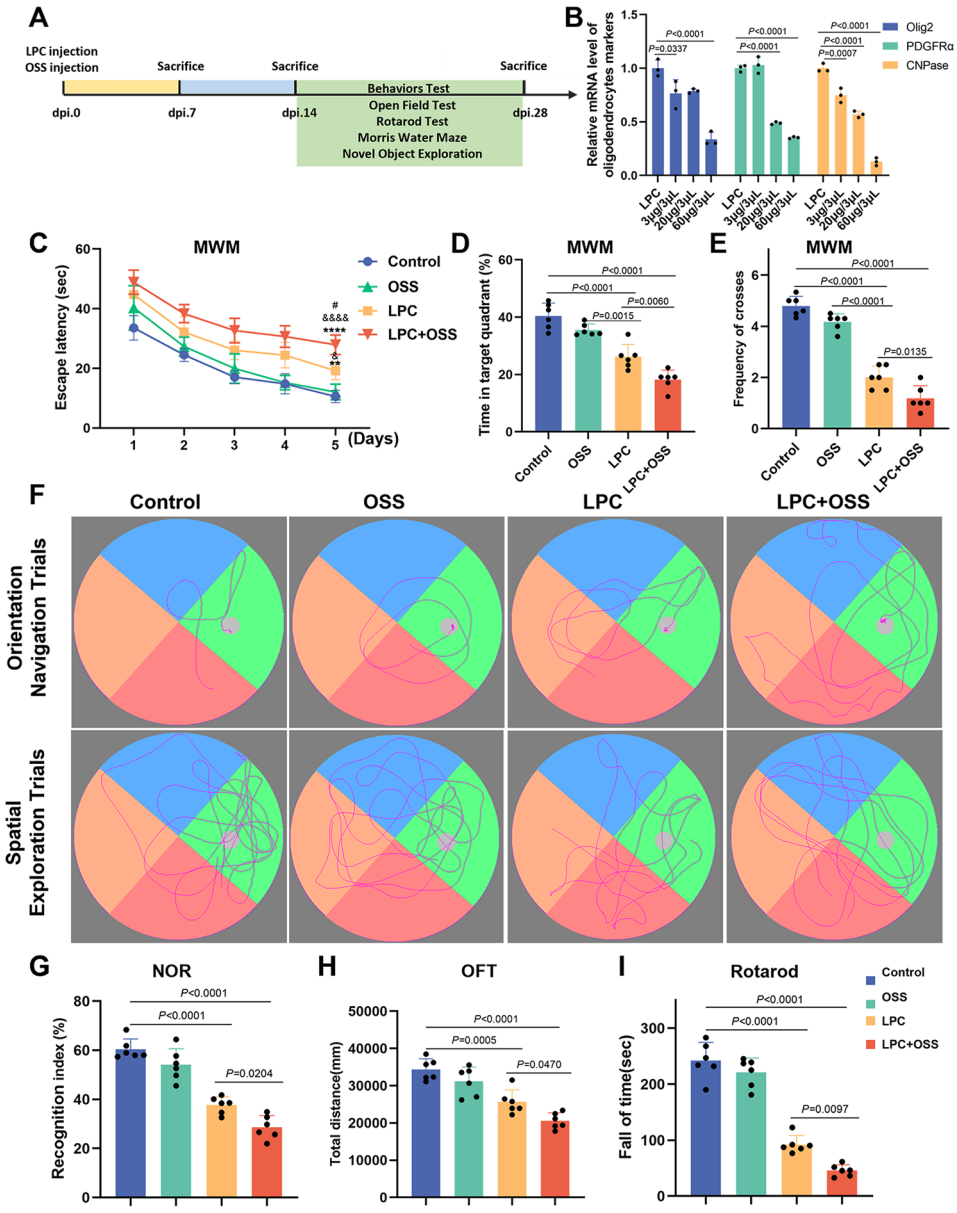

Fig. 2 Behavioral tests on motor and cognitive function of LPC mice with SIRT6 inhibitor treatment **A** Schematics of treatment strategies. The SIRT6 selective inhibitor OSS_128167 was bilaterally injected into the ventricle after LPC injection into CC, and behavioral tests were conducted between 14 ~ 28 dpi. Tissues were collected for histopathological, biochemical analyses at 7, 14, 28 dpi. **B** Olig2, PDGFRα, and CNPase mRNA levels were measured at 14 dpi in demyelinated lesions by qPCR (one-way ANOVA with Tukey's multiple-comparison test, $n = 3$ per group). **C** Escape latencies of the four groups of mice during training days of the Morris water maze (MWM) (two-way ANOVA). **D** Time of mice spent in the target quadrant in the probe trial of the MWM. **E** Number of platform crossings during the probe test in the MWM task. **F** Representative swim trajectories of each group in orientation navigation trials and spatial exploration trials. **G** Preference index of the novel object. **H**, **I** Evaluation of motor function using OFT and Rotarod test in four groups of mice. Statistical analysis was performed using one-way ANOVA and followed by Tukey's multiple comparisons test, $n = 6$ per group. Data: $P < 0.05$ is statistically significant. All values are denoted as the mean ± SD

myelination was greatly reduced in LPC+OSS group relative to that in LPC sections and fluorescent images also demonstrated a decrease of MBP (red) expression in the CC at 7, 14, 28 dpi (Fig. 3A, B; $P<0.0001$, two-tailed t-test). Similar trends were observed in western blotting analysis of myelin associated markers, MOG, MAG and MBP, which showed that levels of all 3 myelin proteins were significantly reduced (Fig. 3C–F; Fig. 3D; $F_{2,9}$ = 91.01, one-way ANOVA; Fig. 3E; $F_{2,9}$ = 22.01, one-way ANOVA ; Fig. 3F; $F_{2.9}$ = 193.0, one-way ANOVA). TEM in the CC showed the percentage of demyelinated axons in LPC+OSS mice was increased compared to LPC ($P<0.0001$) and Control mice ($P<0.0001$) (Fig. 3G; $F_{2,12}$ =168.2, one-way ANOVA). Correspondingly, LPC+OSS

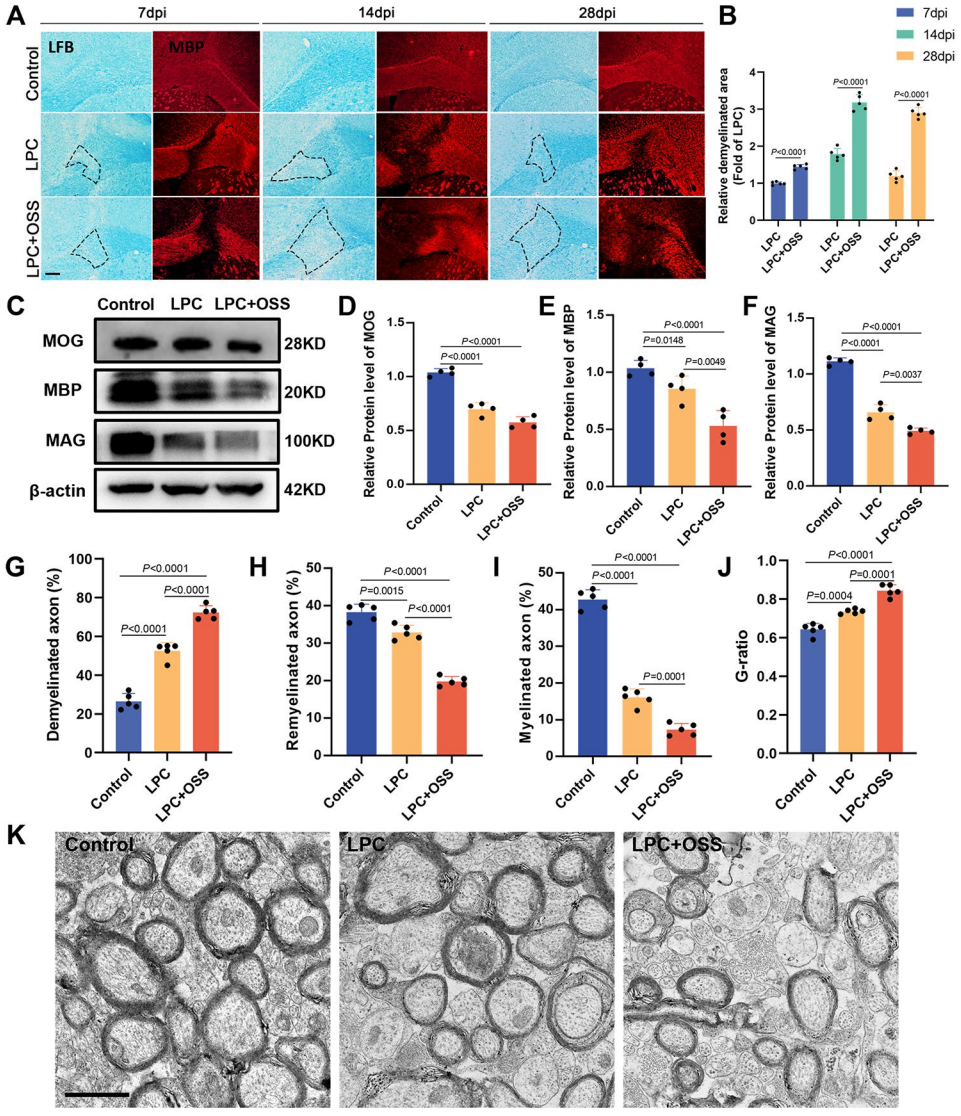

Fig. 3 SIRT6 inhibitor exacerbated white matter damage after LPC **A** Representative images of LFB staining (blue) and MBP immunofluorescence staining (red) in demyelinated lesions at 7, 14, 28 dpi, scale bar = 100 μm. Demyelinated areas were outlined by dashed black lines. **B** Quantification of demyelinated areas of LFB staining (two-tailed unpaired Student's t-test, $n = 5$ per group). **C-F** Western blotting of MOG, MBP, and MAG in Control, LPC and LPC + OSS group (**C**), corresponding statistical analysis for protein expressions of MOG (**D**), MBP (**E**), and MAG (**F**) were shown (one-way ANOVA with Tukey's multiple-comparison test, $n = 4$ per group). **G-K** Representative images of transmission electron microscopy in demyelinated lesions (**K**) and quantification of axons that are myelinated, demyelinated, and remyelinated (%) (**G-I**) and G-ratio (**J**), scale bar = 1 μm (one-way ANOVA with Tukey's multiple-comparison test, $n = 5$ per group). Data: $P < 0.05$ is statistically significant. All values are denoted as the mean ± SD

treated mice contained a smaller proportion of remyelinated axons and myelinated axons scattered throughout the lesion (Fig. 3H; $F_{2,12} = 341.1$, one-way ANOVA; Fig. 3I; $F_{2,12} = 133.6$, one-way ANOVA). Moreover, TEM showed significantly thinner myelin thickness in LPC+OSS mice, with upregulation of G-ratio (the ratio of the inner axonal diameter to the total outer diameter) ($P < 0.0001$ compared with Control group, $P = 0.0001$ compared with LPC group) (Fig. 3J-K; $F_{2,12} = 69.43$, one-way ANOVA). These findings demonstrated that the exacerbation of behavioral abnormalities conferred by SIRT6 inhibition might be due to excessively damaged remyelination.

SIRT6 inhibitor undermined OPCs regeneration after LPC-induced demyelination

After LPC demyelination, responding to the lesion areas molecular signals, OPCs are recruited to the injured area, initiate the regeneration program, and gradually proliferate and differentiate into mature oligodendrocytes with the function of forming myelin sheaths in preparation for remyelination [33]. We next sought to identify the role of SIRT6 on the sequential OPCs regeneration stages,

proliferation and differentiation, after LPC injury. The area where the LPC is injected will show symptoms of demyelination, as shown in Fig. 4A. We therefore quantified the PDGFRα+OPCs in the demyelinated lesions. We found a significant increased ratio of PDGFRα+cells (OPCs marker) of total OLIG2+cells at 7 dpi after LPC injury ($P<0.0001$), indicating OPCs proliferation process was initiated. Whereas the ratio declined when mice subjected OSS_128167 injection in LPC+OSS group, but still above the baseline ($P<0.0001$ compared with LPC group, $P<0.0001$ compared with Control group), suggesting the proliferation was impaired (Fig. 4B, C; $F_{2,12} = 163.8$, one-way ANOVA). The results of radio of CC1+OLIG2+cells (OPCs differentiation marker) of total OLIG2+cells in demyelinated lesions suggested that inhibition of SIRT6 exacerbated OPCs differentiation deficiency, compared with LPC group ($P<0.0001$) (Fig. 4B, D; $F_{2,12} = 60.34$, one-way ANOVA). While, immunofluorescence staining of OLIG2+demonstrated that treatment with OSS alone has no effect on the number of oligodendrocytes (Fig. S3A-B; $P=0.1311$, two-tailed t-test). In addition, as shown in Fig. 4E and F,

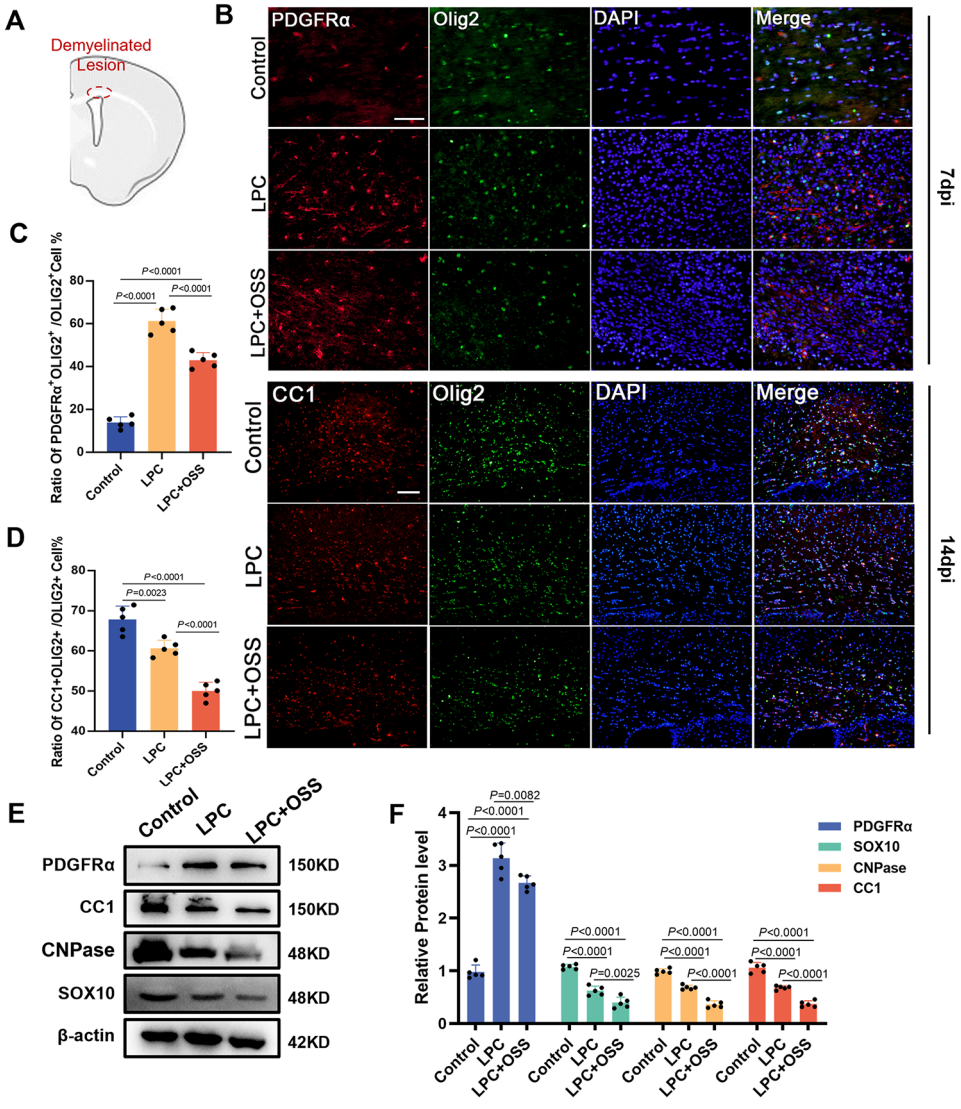

Fig. 4 OPCs regeneration program was impaired with lower proliferation and differentiation in LPC + OSS group **A** Schematic diagram of the demyelinating region after LPC injection. **B** Immunostaining of PDGFRα (red) / OLIG2 (green) / DAPI (blue) at 7 dpi and CC1 (red) / OLIG2 (green) / DAPI (blue) in CC at 14 dpi after LPC injury. PDGFRα: scale bar = 50 μm; CC1: scale bar = 100 μm. **C** Quantitative analysis of PDGFRα and OLIG2 double-positive cells within lesions (one-way ANOVA with Tukey's multiple-comparison test, $n=5$ per group). **D** Quantitative analysis of CC1 relative fluorescence intensity (one-way ANOVA with Tukey's multiple-comparison test, $n=5$ per group). **E**, **F** Representative images for western blotting of PDGFRα, CC1, CNPase, SOX10 and β-actin in Control and LPC-demyelination group treated by PBS or OSS_128167 (**E**), statistical analyses of corresponding protein expressions were shown in **F** (one-way ANOVA with Tukey's multiple-comparison test, $n=5$ per group). Data: $P<0.05$ is statistically significant; one-way ANOVA. All values are denoted as the mean ± SD

the expression levels of markers associated with OPCs regeneration, PDGFRα, CC1, CNPase and SOX10 (OPCs differentiation marker), displayed the similar trends at protein levels (Fig. 4F; $F_{2,12}$ = 86.71, one-way ANOVA). These data indicated that SIRT6 inhibition in LPC demyelination affected the key stages of OPCs regeneration underlying the remyelination.

SIRT6 activator MDL800 promoted remyelination and functional recovery via acetylation modification

MDL800 is a selective allosteric SIRT6 deacetylase activator. The experimental design was as shown in Fig. 5A. Added MDL800 activator studies to the experiment, that MDL800 was administered continuously by intraperitoneal injection (10 mg/kg) for 14 days after LPC injury and behavioral assays and molecular biochemical assays were performed at 14 dpi. Besides major acetylase properties, SIRT6 has been reported to efficiently catalyze the fatty-acid deacylation and ADP-ribosyltransferase activities on substrates [34, 35]. It has not been confirmed whether there is a potential role of OSS_128167 on these two enzyme functions. In order to explore the key role of SIRT6 deacetylation in LPC demyelination, we set up LPC+OSS+MDL group to observe the rescue effect on OSS_128167 inhibition by deacetylase activator MDL800, since the specificity of MDL is well established. Treatment with MDL800 in LPC mice led to a significant increase on expression of remyelination-related markers, MBP, PDGFRα, OLIG2 and CNPase, at mRNA levels (Fig. 5B; $F_{3,8}$ = 19.42, one-way ANOVA; Fig. S4; $F_{3,8}$ = 67.75, one-way ANOVA). Notably, MDL800 treatment markedly declined the acetylation levels of H3K9 (P=0.0072 compared with LPC group) and H3K56 (P=0.0151 compared with LPC group), which are the well-known SIRT6 substrates (Fig. 5C–E; Fig. 5D; $F_{3,8}$ = 88.89, one-way ANOVA; Fig. 5E; $F_{3,8}$ = 54.40, one-way ANOVA). And in LPC+OSS+MDL group, we found that the acetylation levels upregulated by OSS_128167 were reduced by MDL800 (P<0.0001 compared with LPC+OSS group, both of H3K9 and H3K56). Given the enhanced remyelination seen in LPC+MDL group, we focused our analysis on neurobehavioral testing. We first employed the MWM task to assess spatial learning and memory, among the four groups, LPC+MDL group showed a tendency toward shorter escape latency during the acquisition/learning period (Fig. 5F, two-way ANOVA). In the probe test, compared with LPC group, LPC+MDL group also performed improved platform crossover (P=0.0009) and significant preferences for the target quadrant with more time occupation (P=0.0003) (Fig. 5G; $F_{3,20}$ = 18.69, one-way ANOVA; Fig. 5H; $F_{3,20}$ = 32.77, one-way ANOVA). As shown on Fig. 5J, LPC+MDL800 group spent significantly more time on exploring the new object than the familiar one compared to LPC group (P=0.0038), illustrating an improvement in learning performance (Fig. 5J; $F_{3,20}$ = 15.88, one-way ANOVA). And the rescue effect of MDL800 was clearly shown between the LPC+OSS and LPC+OSS+MDL groups. Thereafter, spontaneous locomotor activity was evaluated by OFT, LPC+MDL group traveled the longest distance (Fig. 5K; $F_{3,20}$ = 15.80, one-way ANOVA). The similar results were obtained in Rotarod test, with the longer latency to fall from the rotating rod when LPC+MDL group compared to LPC group (P=0.0163) (Fig. 5L; $F_{3,20}$ = 17.77, one-way ANOVA). Taken together, MDL800 demonstrated excellent therapeutic effect after LPC injury and rescue effects against inhibitor OSS_128167, both molecularly and behaviorally, emphasizing the critical role of SIRT6 acetylation in regulating remyelination.

Inhibition of SIRT6 exacerbated astrocyte activation after LPC injury

To unravel the underlying molecular mechanism of SIRT6 on remyelination following LPC injury, we performed RNA sequencing (RNA-seq) on the mice in four groups, the Control, LPC, LPC+OSS and LPC+MDL groups. And, genes with 2-fold or more significant changes and Q value<0.05 were defined as differentially expressed genes (DEGs). A total of 3252 DEGs were identified, and 1658 and 1594 genes were identified in the following comparison groups: LPC+OSS vs. LPC and LPC+MDL vs. LPC+OSS, respectively (Fig. 6A, B). Notably, 1454 genes overlapped between these two sets of DEGs, indicating a cluster of key genes regulated by SIRT6 on LPC demyelination (Fig. 6C). The Kyoto Encyclopedia of Genes and Genomes (KEGG) analysis of the overlapped 656 DEGs revealed that SIRT6 preferentially affected genes involved in Complement and coagulation cascades, Chemokine signaling pathway, NF-kappa B signaling pathway, Neuroactive ligand-receptor interaction and Cytokine-cytokine receptor interaction, all of which contribute to glial reaction in LPC-demyelinated microenvironment (Fig. 6D). Among the DEGs in above pathway, as shown in heatmap, *C3*, *Tgfb1*, *Gfap*, *Ccl5*, *Tnf*, *Chi3l1*, *Nfkb2* were up-regulated by SIRT6 inhibitor and significantly reversed by MDL800 (Fig. 6E). We also confirmed the reliability of the sequencing results by qPCR (Fig. S5A ; $F_{3,8}$ = 146.8, one-way ANOVA; Fig. S5B ; $F_{3,8}$ = 1549, one-way ANOVA; Fig. S5C; $F_{3,8}$ = 400.7, one-way ANOVA; Fig. S5D; $F_{3,8}$ = 127.0, one-way ANOVA; Fig. S5E ; $F_{3,8}$ = 208.6, one-way ANOVA). We thus further assessed the astrogliosis and microgliosis by immunostaining the brain slices with GFAP and Iba1 in the Control, LPC, LPC+OSS and LPC+MDL groups. The immunofluorescence intensity of GFAP significantly increased in LPC+OSS group, compared with LPC group (P<0.0001). In contrast, the immunofluorescence

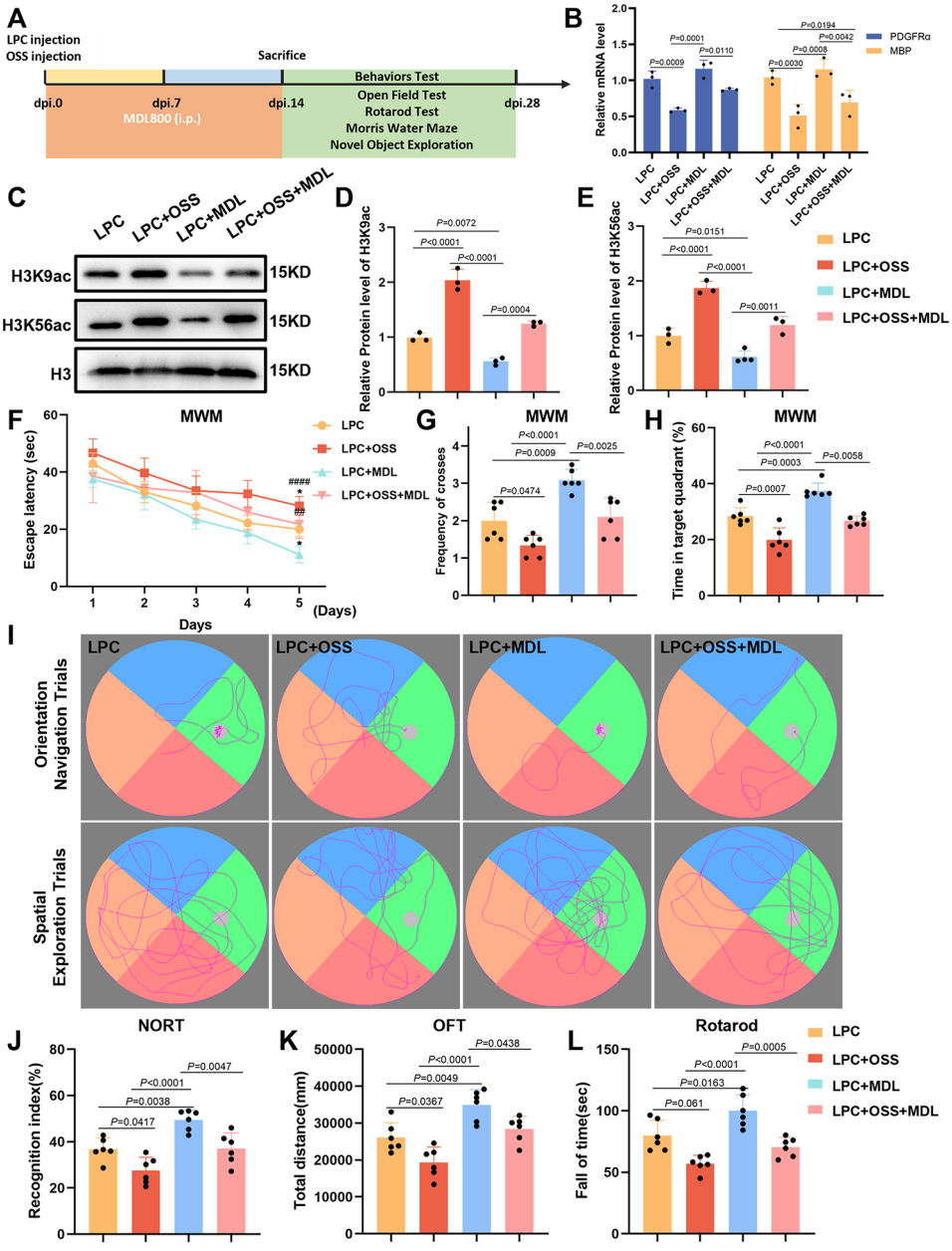

Fig. 5 MDL800 improved remyelination and motor and cognitive impairment **A** Schematics of treatment strategies. Based on above experiment, the MDL treatment group was added. MDL800 was administered continuously by intraperitoneal injection (10 mg/kg) for 14 days after LPC injection, and behavioral tests were conducted between 14 ~ 28 dpi. **B** Quantification of mRNA expressions of remyelination-related markers MBP and PDGFRα (one-way ANOVA with Tukey's multiple-comparison test, $n = 3$ per group). **C-E** Western blotting analysis of SIRT6 substrates H3K9ac and H3K56ac in demyelinated lesions in CC of four groups (**C**), corresponding statistical analysis for H3K9ac (**D**) and H3K56ac (**E**) were shown (one-way ANOVA with Tukey's multiple-comparison test, $n = 3$ per group). **F-I** The MWM test was conducted and representative swim trajectories of each group (**I**). The escape latency at training days 1–5 (**F**) (two-way ANOVA). In the probe test, the number of platform crossings (**G**) and the time spent in target quadrant (**H**) were compared among groups (one-way ANOVA with Tukey's multiple-comparison test, $n = 6$ per group). **J** NOR test measuring the time percentage exploring familiar or new objects (one-way ANOVA with Tukey's multiple-comparison test, $n = 6$ per group). **K** Open field test measuring the distance traveled, and the rotarod challenge of motor ability in four groups (**L**) (one-way ANOVA with Tukey's multiple-comparison test, $n = 6$ per group). Data: $P < 0.05$ is statistically significant. All values are denoted as the mean ± SD

intensity was significantly downregulated after MDL treatment (P=0.0199, compared with LPC group) and even lower than LPC group, close to the baseline value (P=0.0185, compared with Control group) (Fig. 6F and G; $F_{3,16}$ = 120.9, one-way ANOVA). Although the fluorescence intensity trend for Iba1 was similar, astrocytes underwent more dramatic activation compared to microglia in LPC-demyelinated lesions at 14 dpi, in

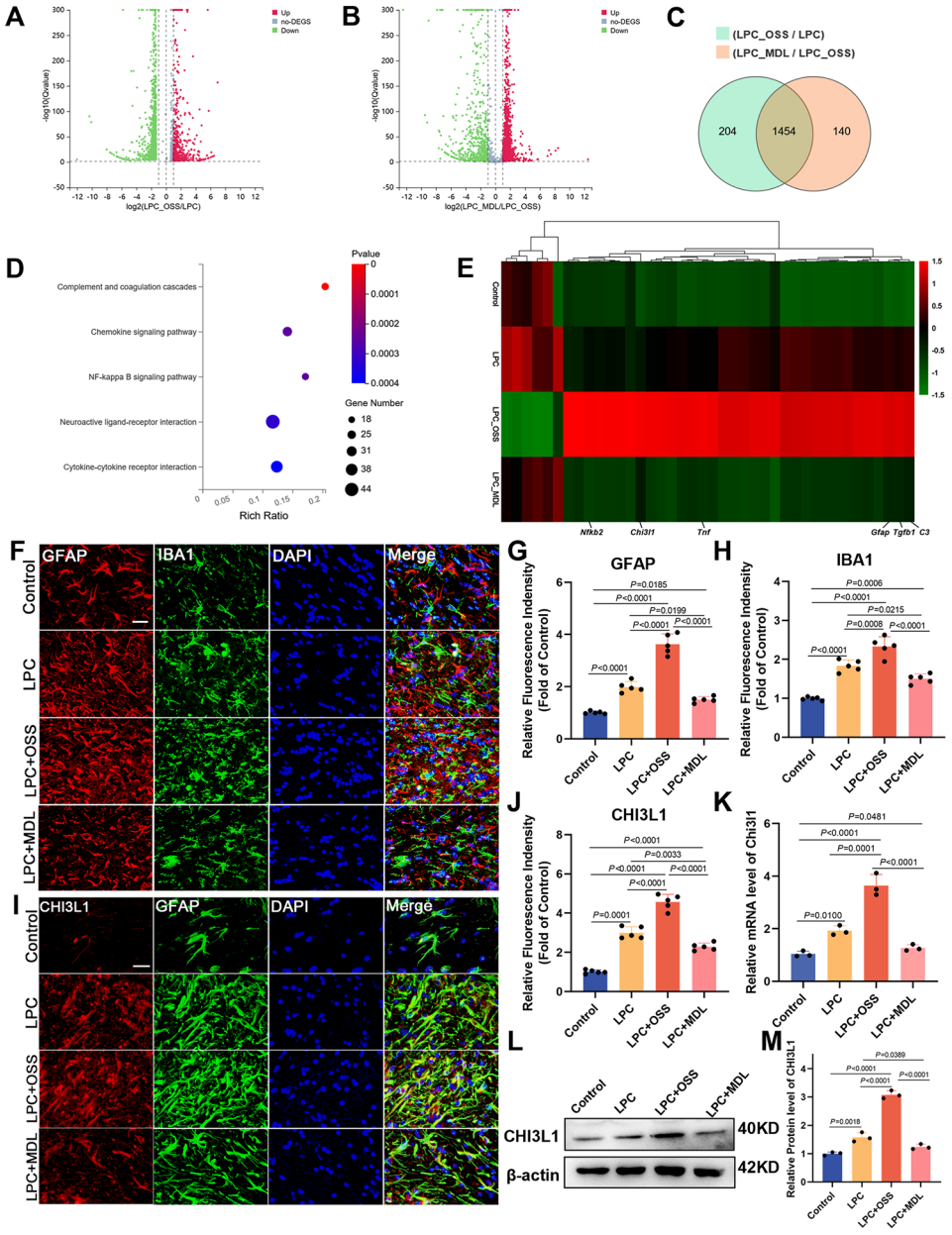

Fig. 6 RNA-sequencing analysis revealed that SIRT6 played critical roles in astrocytes activation in LPC-induced demyelination **A** Volcanic map showed the changes in gene expression in the LPC mice vs. LPC + OSS mice. The threshold was set to |log2 (fold change)| ≥1 and Q value < 0.05. **B** Volcanic map showed the changes in gene expression in the LPC + MDL mice vs. LPC + OSS mice. Green represents downregulation, and red represents upregulation. **C** Venn diagram of DEGs between LPC vs. LPC + OSS and LPC + MDL vs. LPC + OSS. **D** Bubble plots of the KEGG enrichment analysis of overlapped DEGs, and bubble sizes represented the numbers of enriched genes. **E** Heatmap analysis of DEGs associated with the five key pathways among groups, with red represented high expression and green represented low expression for gene expression level. **F-H** Representative immunofluorescence images of astrogliosis and microgliosis (**F**), and quantitative analysis of GFAP positive cells (**G**) and Iba1 positive cells (**H**) (one-way ANOVA with Tukey's multiple-comparison test, $n = 5$ per group). Scale bar = 25 μm. **I** Representative immunofluorescence images of co-localization of CHI3L1 with GFAP. Scale bar = 25 μm. **J** Quantitative analysis of SIRT6 relative fluorescence intensity (one-way ANOVA with Tukey's multiple-comparison test, $n = 5$ per group). **K** CHI3L1 mRNA level was measured at 14 dpi in demyelinated lesions by qPCR (one-way ANOVA with Tukey's multiple-comparison test, $n = 3$ per group). **L-M** Representative images for western blotting of CHI3L1 and β-actin in Control and LPC-demyelination group treated by PBS, OSS_128167 or MDL800 (**L**), statistical analysis of CHI3L1 expressions was shown in **M** (one-way ANOVA with Tukey's multiple-comparison test, $n = 3$ per group). Data: $P < 0.05$ is statistically significant; one-way ANOVA. All values are denoted as the mean ± SD

terms of multiplicity of change (Fig. 6F and H; $F_{3,16}$ = 62.06, one-way ANOVA). Consequently, we focused our attention on astrocytes and found a specific gene *Chi3l1*, encoding an astrocytic secreted glycoprotein, among the key DEGs. In CNS diseases, CHI3L1 was closely associated with reactive astrocytes. Interestingly, immunofluorescence staining also demonstrated substantial co-localization of CHI3L1 with GFAP, with an increase of CHI3L1 expression in mice subjected by OSS_128167 ($P<0.0001$ compared with LPC group), which was reversed by MDL800 administration ($P<0.0001$ compared with LPC+OSS group), consistent with the trend in astrocyte activation (Fig. 6I-J; $F_{3,16}$ = 152.4, one-way ANOVA). The similar results were obtained at mRNA level by qPCR analysis and at protein level by western blot (Fig. 6K; $F_{3,8}$ = 67.75, one-way ANOVA; Fig. 6L-M; $F_{3,8}$ = 176.0, one-way ANOVA). These results indicated that CHI3L1 is involved in SIRT6 regulated astrogliosis during LPC demyelination.

CHI3L1 was critical for SIRT6 to regulate astrocytes phenotypes and function in vitro

It is well established that astrocytes are involved in regulating oligodendrocyte survival and CNS myelination [36, 37]. To determine whether astrocytic SIRT6 had a protective effect on remyelination microenvironment, we first isolated primary astrocytes and OPCs from C57/BL6 mice. LPS treatment was used to induce reactive astrocytes, then we collected the astrocytic conditioned media (AST-CM) in control, LPS, LPS+OSS and LPS+MDL group, as supplements to oligodendrocyte cultures (Fig. 7A). In the immunocytochemistry staining analysis, the number of PDGFRα+OPCs was significantly decreased in LPS+OSS-CM group when compared with LPS-CM treatment, and the analysis of oligodendrocytes maturation indicated that the differentiation of OPCs into mature MBP+oligodendrocytes was inhibited, whereas MDL800 treatment partially rescued OPCs regeneration (Fig. 7B–E; Fig. 7B; $F_{3,16}$ = 29.55, one-way ANOVA; Fig. 7C; $F_{3,16}$ = 34.05, one-way ANOVA; Fig. 7D; $F_{3,16}$ = 69.21, one-way ANOVA). Based on immunocytochemistry staining, the Sholl analysis revealed that oligodendrocytes in LPS+OSS-CM group exhibited decreased intersection numbers with the concentric circles, indicating the differentiation complexity impairment. In contrast, MDL800 altered this decrease (Fig. 7F, G, two-way ANOVA). As reported, astrocytes have been roughly categorized into A1 (neurotoxic; pro-inflammatory) and A2 (neuroprotective; anti-inflammatory) phenotypes, closely related to cell functions [38]. We then examined the effects of SIRT6 on astrocytes phenotypes in above four groups. As shown in Fig. 7H and I, C3 (A1 astrocytes marker) displayed markedly increased on mRNA level in qPCR analysis in the comparison of LPS+OSS and LPS ($P=0.0001$), and with MDL800 treatment, the expression restored to the baseline ($P<0.0001$)(Fig. 7H; $F_{3,8}$ = 185.7, one-way ANOVA). However, no significant difference was detected in S100a10 (A2 astrocytes marker) (Fig. 7I; $F_{3,8}$ = 2.604, one-way ANOVA). The above results indicated that SIRT6 specifically upregulated the A1 neurotoxicity astrocytes phenotype, not the A2 phenotype. Further, we verified the regulation of SIRT6 on CHI3L1 in vitro. Firstly, qPCR results showed that SIRT6 negatively regulated CHI3L1 expression in LPS-induced reactive astrocytes. Inhibition of SIRT6 markedly increased CHI3L1 mRNA levels, whereas activation of SIRT6 rescued this change (Fig. 7J; $F_{3,8}$ = 116.6, one-way ANOVA). Besides, astrocytes were transfected with CHI3L1 siRNA and CHI3L1 deficiency attenuated the upregulation in C3 expression caused by SIRT6 inhibitor (Fig. S6A; $F_{3,8}$ = 93.27, one-way ANOVA; Fig. S6B; $F_{3,8}$ = 67.21, one-way ANOVA; Fig. S6C; $F_{3,8}$ = 3.25, one-way ANOVA). We then performed chromatin immunoprecipitation (ChIP) assays for acetyl H3K9, the specific deacetylation downstream site of SIRT6, in astrocytes treated with LPS or LPS+OSS. As shown in Fig. 7K, ChIP assay confirmed that H3K9 acetylation occupancy on the CHI3L1 promoter was enhanced with OSS_128167 inhibition of SIRT6 ($P<0.0001$, compared with LPS). Hence, we hypothesized that SIRT6 regulates CHI3L1 expression by modulating the extent of H3K9ac enrichment. To sum up, these data illustrated that SIRT6 specifically regulated A1 astrocyte activation and CHI3L1 was a critical downstream gene mediated by SIRT6 deacetylation.

Astrocytic SIRT6/CHI3L1 regulated remyelination and functional recovery in LPC mice

Having observed that inhibition of SIRT6 exacerbated astrocyte activation and impaired remyelination in LPC mice, we next asked whether overexpression SIRT6 in astrocytes would have therapeutic effects. We then validated the effects of astrocytic SIRT6/CHI3L1 on remyelination in vivo. 5 days before LPC treatment, mice were stereotaxically injected with the AAV9 into the corpus callosum, inducing astrocyte-specific GFaABC1D promoter-driven SIRT6 overexpression or CHI3L1 overexpression (Fig. 8A and Fig. S7A). Subsequently, behavioral assays were conducted at 14 dpi after LPC injury. In the MWM test, LPC-induced cognitive dysfunction was significantly dampened in the mice injected with the AAV-SIRT6-OE, with shorter escape latency in learning stage, improved platform crossover and more time occupation in target quadrant in the probe test (Fig. 8B-D; Fig. 8C; $F_{3,20}$ = 15.69, one-way ANOVA; Fig. 8D; $F_{3,20}$ = 14.12, one-way ANOVA). And motor function was analyzed by Rotarod test, and AAV-SIRT6OE treatment also showed good therapeutic effects, compared with LPC mice (Fig. 8E; $F_{3,20}$ = 84.45,

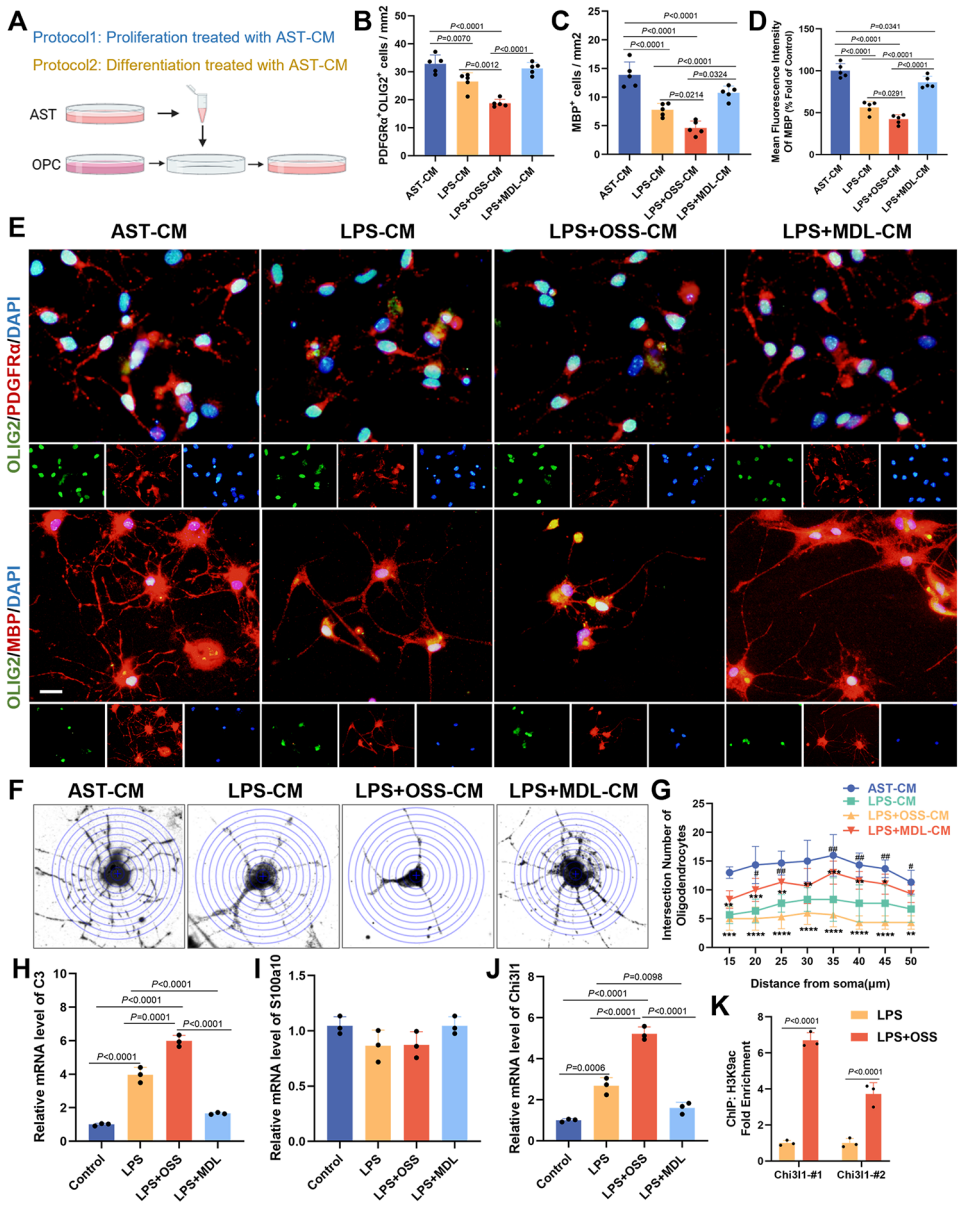

Fig. 7 SIRT6 regulated astrocytes phenotypes and function in vitro **A** Experimental protocol diagram. Primary astrocytes were used to collect AST-CM with PBS, LPS, LPS + OSS or LPS + MDL, as supplements to primary OPCs cultures in proliferation or differentiation stages. **B-E** Representative immunofluorescence images of PDGFRα (red) / OLIG2 (green) / DAPI (blue) and MBP (red) / OLIG2 (green) / DAPI (blue) (**E**), and quantitative analysis of PDGFRα and OLIG2 double-positive cells (**B**) and MBP positive cells (**C**, **D**) (one-way ANOVA with Tukey's multiple-comparison test, $n = 5$ per group). Scale bar = 20 μm. **F** Representative MBP-labeled oligodendrocytes were reconstructed for Sholl analysis with superimposed concentric circles at 5 μm intervals. **G** Intersection numbers with the concentric circles were shown among groups. **H-J** Quantification of mRNA expressions of C3, S100a10 and CHI3L1 in primary astrocytes among groups (one-way ANOVA with Tukey's multiple-comparison test, $n = 3$ per group). **K** ChIP assay was performed to detect the enrichment of H3K9ac at the gene promoter regions of CHI3L1 (two-tailed unpaired Student's t-test, $n = 3$ per group). Data: $P < 0.05$ is statistically significant. All values are denoted as the mean ± SD

one-way ANOVA). Notably, the therapeutic effects on functional recovery of astrocytic SIRT6 were reversed by AAV-CHI3L1OE injection, which confirmed that CHI3L1 is indeed an important downstream target for astrocytic SIRT6. Then, we assessed the demyelinated lesions in LPC, LPC+AAV-SIRT6OE and LPC+AAV-SIRT6OE+AAV-CHI3L1OE groups. LFB staining results demonstrated AAV-SIRT6OE reduced the area of demyelination, compared with LPC group ($P<0.0001$), whereas AAV-CHI3L1OE injection undermines therapeutic effect ($P<0.0001$, compared with LPC+AAV-SIRT6OE group) (Fig. 8G-H; Fig. 8H; $F_{2,12} = 101.7$, one-way ANOVA). TEM cross sections confirmed this conclusion (Fig. S8). AAV-SIRT6OE reduced demyelination injury induced

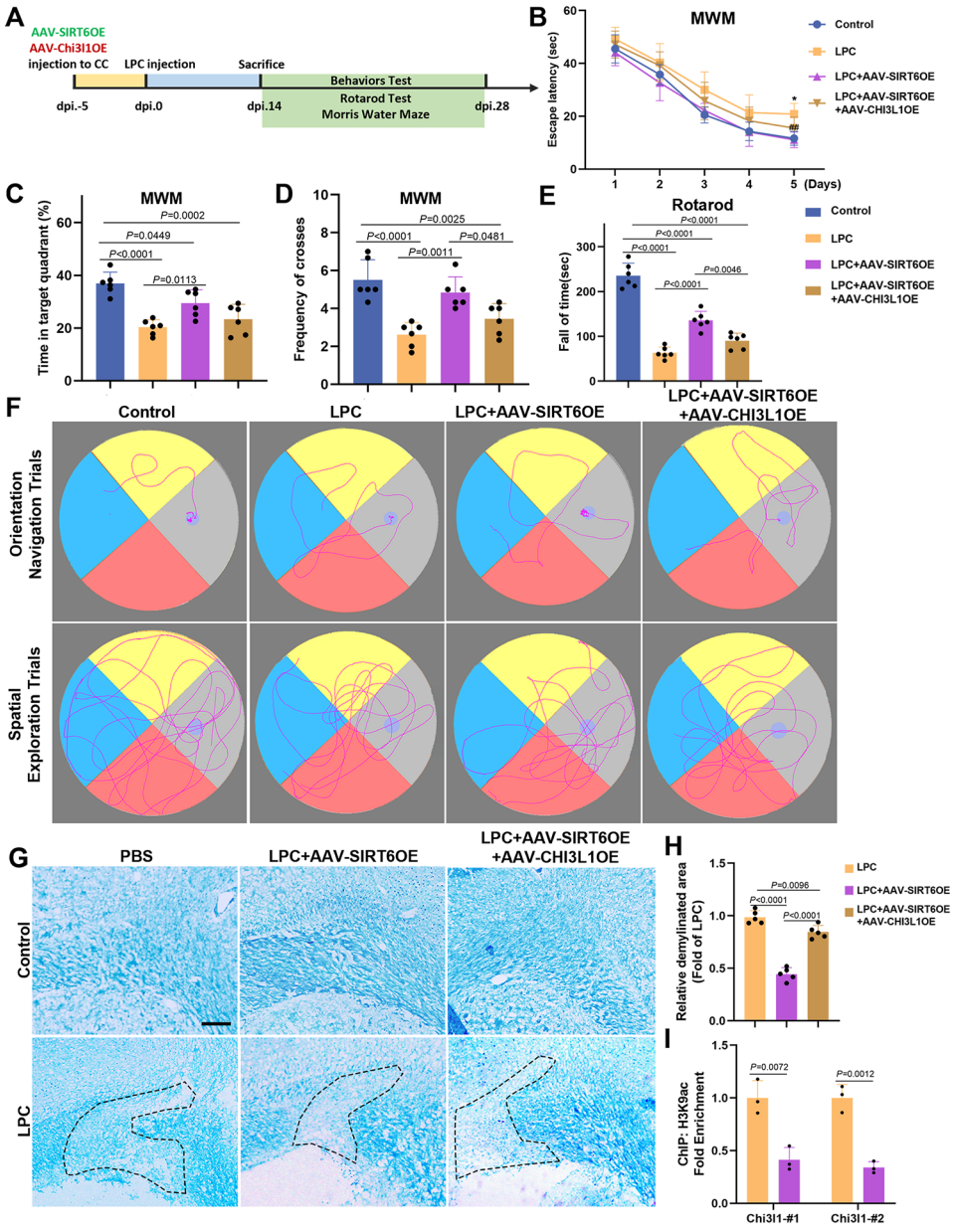

Fig. 8 SIRT6 regulated remyelination and functional recovery via CHI3L1 in LPC induced demyelination **A** Schematics of treatment strategies. Transfection of astrocytes with AAV9 inducing astrocyte-specific GFaABC1D promoter-driven SIRT6 overexpression or CHI3L1 overexpression, with stereotaxical injection into CC, 5 days prior to exposure to LPC injuries in 8-week-old C57BL/6 mice. Behavioral tests were conducted between 14 ~ 28 dpi. Tissues were collected for histopathological, biochemical analyses at 14 dpi. **B-D** The MWM test was conducted. The escape latency at training days 1–5 (**B**) (Two-way ANOVA). In the probe test, the time spent in target quadrant (**C**) and the number of platform crossings (**D**) were compared among groups (one-way ANOVA with Tukey's multiple-comparison test, $n = 6$ per group). **E** Rotarod test (one-way ANOVA with Tukey's multiple-comparison test, $n = 6$ per group). **F** Representative swim trajectories of each group in orientation navigation trials and spatial exploration trials. **G** Representative images of LFB staining (blue) in demyelinated lesions in Control and LPC mice treated by PBS, AAV-SIRT6OE or AAV-SIRT6OE + AAV-CHI3L1OE, scale bar = 100 μm. **H** Statistical analysis for demyelinated areas (one-way ANOVA with Tukey's multiple-comparison test, $n = 5$ per group). **I** ChIP-qPCR analysis to determine the histone acetylation of CHI3L1 promoter in AAV infected CC (two-tailed unpaired Student's t-test, $n = 3$ per group). Data: $P < 0.05$ is statistically significant. All values are denoted as the mean ± SD

by LPC, while AAV-CHI3L1OE injection reversed the improvement effect of SIRT6. At last, we performed ChIP assays on corpus callosum tissue for acetyl H3K9 in LPC mice injected with AAV-SIRT6OE or AAV-sham. The levels of H3K9 acetylation in the CHI3L1 promoter were significantly reduced upon SIRT6 overexpression (Fig. 8I; Chi3l1-#1, $P=0.0072$, two-tailed t-test; Chi3l1-#2, $P=0.0012$, two-tailed t-test). Altogether, these findings identified that astrocytic SIRT6 was sufficient to modulate remyelination and AAV-SIRT6OE served as a

candidate therapy to restore remyelination microenvironment, by alleviating CHI3L1 expression anomalies in reactive astrocytes.

Discussion

Demyelinating diseases of the CNS broadly consist of impaired myelin formation and myelin destruction, whereas abnormalities in the lesion microenvironment are important in preventing remyelination, such as MS, which is characterized by neuroinflammation, demyelination and progressive neurological deterioration [39, 40]. In this study, we explored the role of SIRT6 in the demyelinating disease by constructing the LPC model simulating the focal lesions in MS, and found that SIRT6 was crucial for the progression of remyelination by mediating glial activation in lesion microenvironment. And for the first time, we confirmed the positive role of astrocytic SIRT6/CHI3L1 in remyelination and neurological function recovery.

MS is the most prevalent demyelinating neurodegenerative disease affecting young adults, characterized by neuroinflammation in the central nervous system (CNS) [41]. MS exhibits significant sex differences in many ways, for example in astrocyte activation [42, 43]. It has been reported complement component 3 (C3) has a greater increase in optic nerve astrocytes in female EAE model versus healthy females, as compared to that in male EAE versus healthy males. And high expression of C3 is related to worse retinal ganglion cell (RGC) and axonal loss in EAE females [44]. In CNS, besides MS, sex differences in astrocyte also exist in chronic stress-induced morphological changes across multiple brain regions and hippocampal memory [45, 46]. Notably, sex-associated CHI3L1 has been reported in Alzheimer's disease and is associated with memory performance and brain Aβ deposition [47, 48]. In our study, sex-dependent astrocyte reactivity might be an important sight to explore SIRT6/CHI3L1 in demyelinated diseases. We chose female mice to follow the tendency in MS, which is more prevalent in females, but as mentioned above, the pathogenesis of MS in females and males may be different, which is a study limitation.

SIRT6 has been confirmed to play important roles in multiple diseases, including AD, Parkinson's disease (PD), ischemic stroke and Spinal Cord Injury. Although the critical roles of SIRT6 in CNS diseases have been progressively identified, the role of SIRT6 in demyelinating diseases remains unclear. In our study, we reported the regulation of SIRT6 in remyelination in LPC mice for the first time. LPC mice is a well-established experimental model that allows the study of the de- and remyelination on the same model in a relatively short period of time. Our work suggested that the SIRT6 inhibitor, OSS_128167, markedly inhibited remyelination and caused damage to neurological functions, whereas when treatment with MDL800, the inhibitory phenotype of OSS_128167 was rescued. Notably, the excellent therapeutic effects were exhibited when MDL800 administered alone against LPC injury, from which, we hypothesized that SIRT6 might be a key target as remyelination regulator and potential therapeutic in demyelinating diseases. Similarly, we demonstrated the therapeutic effect of SIRT6 on LPC demyelination via AAV transfection in the final animal experiment part. In clinical therapy, the application of AAV is limited due to certain risks, while recent studies have shown that natural compounds can be used as modulators of SIRT6 for diseases treatment [49, 50]. Among them, Isoquercetin and Delphinidin act as sirt6 activators, which produce antioxidant activity through scavenging of ROS to against aging and inflammation [51, 52]. Thus, it is suggested that related natural compounds as SIRT6 modulators might provide a promising strategy for treatment of demyelinating diseases.

Glial cells in the lesion microenvironment are involved in the maintenance and repair of myelin; alterations in astrocytes and microglia facilitate demyelination and disrupt the processes of remyelination [33, 53]. Our RNA-seq analysis showed that among the up-regulated DEGs, besides inflammatory signaling pathway and chemokines, a significant up-regulation of complement signaling was detected, such as C3 and C1q. C3 is secreted by astrocytes as a signal to activate microglial cells, while activated microglia can also induce A1 astrocytes phenotype through the secretion of C1q, indicating that after SIRT6 inhibition, the glial complexities are aggravated in the demyelinated environment [54, 55]. Consequently, there is an urgent need to identify key cell types and targets to elucidate this complex environment. Based on RNA-seq analysis, we validated the role of SIRT6 on glial cell. By comparing the activation of astrocytes and microglia, we found a significant activation of astrocytes at 14 dpi, the peak of SIRT6 expression during demyelination, suggesting that astrocytes might be the crucial cell type regulated by SIRT6. Together with other cellular elements of the CNS, reactive astrocytes play the important roles in the modulation of neuroinflammation. And previous studies have reported that astrocytes presented a mixed inflammatory and neuroprotective signature during remyelination, as A1 and A2 phenotypes, promoting further damage or contributing to repair [36]. Our in vivo and in vitro data further showed that SIRT6 had a predisposition in regulating reactive astrocytes phenotypes in LPC mice, which indicated SIRT6 was an important regulator of dichotomous processes on astrocytes function, with more tendency on A1. We also found that SIRT6 is also expressed in the microglia, while microglial activation is closely related to inflammatory damage. For

instance, the pharmacological activation of Sirt6 ameliorates neuroinflammation and attenuates brain injury in mice with ischemic stroke [56]. It also opens up several important issues that are worth studying in the future.

Our work showed the importance of microenvironment-oligodendrocyte interactions in remyelination, and we have tried to find a key molecule to regulate the relationship between the two. CHI3L1, an astrocytic specific secreted glycoprotein in the CNS, was shown to be significantly higher in mRNA expression after SIRT6 inhibition based on RNA-seq analysis. We were curious whether there is a SIRT6-CHI3L1 stream in regulating astrocytic function and participating in remyelination after LPC injury. CHI3L1 is primarily associated with reactive astrocytes in a variety of diseases, such as AD, MS, TBI and gliomas [15, 16, 18]. In our study, in the LPC model after SIRT6 treatment, the changes in demyelination injury, CHI3L1 and the activation of A1 astrocytes were consistent in fluorescent staining and qPCR assay, suggested CHI3L1 might be the key molecular. In previous studies, CHI3L1 has been known as a reliable biomarker, with mostly positively correlation with the degree of disease progression [14, 16]. While, Chi3l1-knockout mice showed higher infarct volumes and lower neurological deficit scores 24 h after ischemia/reperfusion, with significantly increased expression of inflammation-related proteins, compared with wild-type mice [19]. This suggested that CHI3L1 needed to maintain a range of expression in neurological diseases, not simply "use it or lose it". And our study revealed that astrocytic SIRT6 might be the key to achieve this regulation. Based on the results of the negative correlation between SIRT6 and CHI3L1, we verified the direct regulation of CHI3L1 by SIRT6 mediated histone H3K9ac deacetylation using ChIP assays in vivo and in vitro. Notably, in LPC mice, astrocyte specific AAV-CHI3L1OE was able to partially counteract the therapeutic effects of astrocyte specific AAV-SIRT6OE in remyelination and neurological function improvement, reconfirming CHI3L1 as a downstream of SIRT6 in myelin repair. The above results provided direct evidence for the critical regulatory role of astrocytic SIRT6/CHI3L1 in remyelination. A newly published article reporting the role of astrocyte-derived CHI3L1 signaling in the demyelinated hippocampus supported our findings, although this article focused on the effects of injury environment on neurogenesis [57]. In addition to CHI3L1, the research on SIRT6 and Notch signaling is also a novel field in oligodendrocytes. It has been reported that Notch proteins are transmembrane proteins activated by ligands such as Jagged1, which participate in cell proliferation, differentiation, and apoptosis processes in a cell context–dependent manner. In CNS, Notch signaling promotes the differentiation of most glial cell subtypes, but inhibits oligodendrocyte maturation. And for current reports on SIRT6, in prostate cancer studies, increased mRNA levels of receptors and ligands in the Notch pathway were shown in cells stably overexpressing SIRT6 [58]. In ischemic stroke, SIRT6 inhibited Notch signaling via suppressing Notch1 and ameliorated MCAO/R-induced brain damage [59]. The role of SIRT6 and Notch in regulating oligodendrocyte fate deserves further investigation in the subsequent experiments.

However, there were some limitations in this part, that we did not provide evidence of potential receptors for CHI3L1 on OPCs. Whereas, based on previous studies, IL-13 receptor α2 (IL-13Rα2), transmembrane protein 219 (TMEM219), and chemoattractant receptor homologous with T helper 2 cell (CRTH2) have been reported as CHI3L1 receptors to mediate its effect [60]. Li et al. found astrocytic CHI3L1 regulated OPCs proliferation via OPCs surface receptor CRTH2 in AxD [21]. While more experiments are needed to confirm whether CRTH2 is a downstream target of CHI3L1 on OPCs in LPC model, for above study also provides us with a direction. Furthermore, the validation of SIRT6 direct effects on oligodendrocytes has been lacking, although RNA-seq suggested a role for SIRT6 in regulating the glial environment. Zou et al. found that, during peripheral nerve regeneration, SIRT6 regulated Schwann cells dedifferentiation via c-Jun pathway and also promoted macrophages polarized into M2 type, in which Schwann cells were key for remyelination of peripheral nerves, with a function similar to that of oligodendrocytes in CNS [61, 62]. However, as the reporter suggested, in their follow-up studies, SIRT6 conditional knockout mice in Schwann cells or macrophages were critical to reveal the roles of SIRT6 in peripheral nerve regeneration and underlying mechanisms [61]. For us, explaining the cell-type-specific regulation of SIRT6 in this complex lesion environment, conditional knockout mice are also necessary. In subsequent experiments, we will attempt to use conditional knockout mice for more refined studies.

We used reactive astrocytes conditioned media to validate the effect of SIRT6 in vitro, and found that conditioned media from reactive astrocytes treated with SIRT6 inhibitor exacerbated the dysregulation of OPCs regeneration, whereas MDL800 treatment demonstrated therapeutic effects. It should be noted here that, unlike animal experiments, LPS treatment deprived the astrocyte supportive effects on OPCs, with reduced OPCs number. In LPC mice, as reported in several studies, we found that OPCs were activated by acute injury-induced changes in lesion environment, producing the rapid proliferative response to demyelinating injury [63, 64]. Obviously, the difference in proliferation of OPCs in vivo and in vitro was not caused by LPS or LPC, because reactive proliferation of OPCs was also observed in LPS-induced neonatal white matter injury [64–66]. This might be related

to the dose and duration of LPS, as well as single cell type culture environment, resulting in different degrees of activation of astrocytes. These differences required more experiments to resolve.

Conclusions

In conclusion, our study is the first to report the critical role of SIRT6 in LPC-induced demyelination and the specific mechanism in regulating CHI3L1 expression in astrocyte via SIRT6-dependent histone deacetylation. Our findings clarify the mechanism of SIRT6 mediated remyelination microenvironment and provide a promising strategy for the treatment of MS.

Abbreviations

AAV	Adeno-associated virus
AxD	Alexander disease
AD	Alzheimer's disease
ANOVA	Analysis of variance
AST-CM	Astrocytic conditioned media
CNS	Central nervous system
CHI3L1	Chitinase-3–like protein 1
ChIP	Chromatin immunoprecipitation
CC	Corpus callosum
Dpi	Days post injury
DEGs	Differentially expressed genes
GFAP	Glial fibrillary acidic protein
H3K56Ac	Histone-H3-lysine-56 acetylation
H3K9Ac	Histone-H3-lysine-9 acetylation
KEGG	Kyoto Encyclopedia of Genes and Genomes
LFB	Luxol Fast Blue
LPC	Lysolecithin
LPS	Lipopolysaccharide
MWM	Morris water maze
MS	Multiple sclerosis
NOR	Novel object recognition
OPCs	Oligodendrocyte precursor cells
OFT	Open Field Test
RNA-seq	RNA sequencing
SIRT6	Sirtuin6
TEM	Transmission electron microscopy

Supplementary Information

The online version contains supplementary material available at https://doi.org/10.1186/s12974-024-03241-1.

Supplementary Material 1

Acknowledgements

We would like to thank the staff of the electron microscopy laboratory of the Morphological Experimental Center in the School of Basic Medical Sciences, Cheeloo College of Medicine, for technical assistance.

Author contributions

JD designed and performed the majority of the research work; YY performed experiments and tissue harvesting; DW, TZ, FP and NL contributed to data collection and behavioral tests; LW and JS contributed to TEM experiments; DW, LK and CD analyzed data/statistical analysis; WZ and AH were involved in conception and design, manuscript writing and final approval of the manuscript.

Funding

This study was supported by funding from the National Natural Science Foundation of China (No. 82071267 and 82371179), Foundation of Jinan (No. 2021GXRC103).

Data availability

No datasets were generated or analysed during the current study.

Declarations

Ethics approval and consent to participate

Animal protocols have been approved by the Animal Care and Utilization Committee of Shandong University and were performed according to the Guide for the Care and Use of Laboratory Animals of the National Institutes of Health of the United States.

Consent for publication

Not applicable.

Competing interests

The authors declare no competing interests.

Received: 17 June 2024 / Accepted: 23 September 2024
Published online: 28 September 2024

References

1. Woo MS, Engler JB, Friese MA. The neuropathobiology of multiple sclerosis. Nat Rev Neurosci. 2024;25(7):493–513.
2. Højsgaard Chow H, Schreiber K, Magyari M, Ammitzbøll C, Börnsen L, Romme Christensen J, et al. Progressive multiple sclerosis, cognitive function, and quality of life. Brain Behav. 2018;8(2):e00875.
3. Bachmann H, Vandemoortele B, Vermeirssen V, Carrette E, Vonck K, Boon P, Raedt R, et al. Vagus nerve stimulation enhances remyelination and decreases innate neuroinflammation in lysolecithin-induced demyelination. Brain Stimul. 2024;17(3):575–87.
4. McMurran CE, Zhao C, Franklin RJM. Toxin-based models to investigate demyelination and remyelination. Methods Mol Biol. 2019;1936:377–96.
5. Korotkov A, Seluanov A, Gorbunova V. Sirtuin 6: linking longevity with genome and epigenome stability. Trends Cell Biol. 2021;31(12):994–1006.
6. Guo Z, Li P, Ge J, Li H. SIRT6 in aging, metabolism, inflammation and Cardiovascular diseases. Aging Dis. 2022;13(6):1787–822.
7. Ferrara G, Benzi A, Sturla L, Marubbi D, Frumento D, Spinelli S, et al. Sirt6 inhibition delays the onset of experimental autoimmune encephalomyelitis by reducing dendritic cell migration. J Neuroinflammation. 2020;17(1):228.
8. Kaluski S, Portillo M, Besnard A, Stein D, Einav M, Zhong L, et al. Neuroprotective functions for the histone deacetylase SIRT6. Cell Rep. 2017;18(13):3052–62.
9. Song MY, Yi F, Xiao H, Yin J, Huang Q, Xia J, et al. Energy restriction induced SIRT6 inhibits microglia activation and promotes angiogenesis in cerebral ischemia via transcriptional inhibition of TXNIP. Cell Death Dis. 2022;13(5):449.
10. He T, Shang J, Gao C, Guan X, Chen Y, Zhu L, et al. A novel SIRT6 activator ameliorates neuroinflammation and ischemic brain injury via EZH2/FOXC1 axis. Acta Pharm Sin B. 2021;11(3):708–26.
11. Portillo M, Eremenko E, Kaluski S, Garcia-Venzor A, Onn L, Stein D, et al. SIRT6-CBP-dependent nuclear tau accumulation and its role in protein synthesis. Cell Rep. 2021;35(4):109035.
12. Jing S, Wang X, Zhang Z, Cao D, Huang K, Wang Y, et al. Hesperetin attenuates cognitive dysfunction via SIRT6/NLRP3 pathway in scopolamine-induced mice. Metab Brain Dis. 2023;38(7):2443–56.
13. Hu K, Chen H, Gao Y, Hua R, Shi X, Li L, et al. Astrocytic SIRT6 is a potential anti-depression and anti-anxiety target. Prog Neuropsychopharmacol Biol Psychiatry. 2023;123:110702.
14. Li F, Liu A, Zhao M, Luo L. Astrocytic Chitinase-3-like protein 1 in neurological diseases: potential roles and future perspectives. J Neurochem. 2023;165(6):772–90.
15. Lananna BV, McKee CA, King MW, Del-Aguila JL, Dimitry JM, Farias FHG, et al. *Chi3l1*/YKL-40 is controlled by the astrocyte circadian clock and regulates neuroinflammation and Alzheimer's disease pathogenesis. Sci Transl Med. 2020;12(574):eaax3519.
16. Cubas-Núñez L, Gil-Perotín S, Castillo-Villalba J, López V, Solís Tarazona L, Gasqué-Rubio R, et al. Potential role of CHI3L1 + astrocytes in Progression in MS. Neurol Neuroimmunol Neuroinflamm. 2021;8(3):e972.
17. Vu L, An J, Kovalik T, Gendron T, Petrucelli L, Bowser R. Cross-sectional and longitudinal measures of chitinase proteins in amyotrophic lateral sclerosis

and expression of CHI3L1 in activated astrocytes. J Neurol Neurosurg Psychiatry. 2020;91(4):350–8.
18. Hai L, Hoffmann DC, Wagener RJ, Azorin DD, Hausmann D, Xie R, et al. A clinically applicable connectivity signature for glioblastoma includes the tumor network driver CHI3L1. Nat Commun. 2024;15(1):968.
19. Im JH, Yeo IJ, Park PH, Choi DY, Han SB, Yun J, et al. Deletion of Chitinase-3-like 1 accelerates stroke development through enhancement of Neuroinflammation by STAT6-dependent M2 microglial inactivation in Chitinase-3-like 1 knockout mice. Exp Neurol. 2020;323:113082.
20. Olabarria M, Goldman JE. Disorders of astrocytes: Alexander Disease as a model. Annu Rev Pathol. 2017;12:131–52.
21. Li L, Tian E, Chen X, Chao J, Klein J, Qu Q, et al. GFAP mutations in astrocytes impair oligodendrocyte progenitor proliferation and myelination in an hiPSC model of Alexander Disease. Cell Stem Cell. 2018;23(2):239–e2516.
22. Wang Y, Sadike D, Huang B, Li P, Wu Q, Jiang N, et al. Regulatory T cells alleviate myelin loss and cognitive dysfunction by regulating neuroinflammation and microglial pyroptosis via TLR4/MyD88/NF-κB pathway in LPC-induced demyelination. J Neuroinflammation. 2023;20(1):41.
23. Jin J, Li W, Wang T, Park BH, Park SK, Kang KP. Loss of Proximal Tubular Sirtuin 6 aggravates unilateral Ureteral obstruction-Induced Tubulointerstitial inflammation and fibrosis by regulation of β-Catenin acetylation. Cells. 2022;11(9):1477.
24. Zhang J, Li Y, Liu Q, Huang Y, Li R, Wu T, et al. Sirt6 alleviated liver fibrosis by Deacetylating Conserved Lysine 54 on Smad2 in hepatic stellate cells. Hepatology. 2021;73(3):1140–57. https://doi.org/10.1002/hep.31418. Epub 2020 Nov 10. PMID: 32535965; PMCID: PMC8048913.
25. Xie D, Ge X, Ma Y, Tang J, Wang Y, Zhu Y, et al. Clemastine improves hypomyelination in rats with hypoxic-ischemic brain injury by reducing microglia-derived IL-1β via P38 signaling pathway. J Neuroinflammation. 2020;17(1):57.
26. Li J, Xu P, Hong Y, Xie Y, Peng M, Sun R, et al. Lipocalin-2-mediated astrocyte pyroptosis promotes neuroinflammatory injury via NLRP3 inflammasome activation in cerebral ischemia/reperfusion injury. J Neuroinflammation. 2023;20(1):148.
27. Zou Y, Zhang J, Liu J, Xu J, Fu L, Ma X, et al. SIRT6 negatively regulates Schwann cells dedifferentiation via targeting c-Jun during Wallerian Degeneration after Peripheral nerve Injury. Mol Neurobiol. 2022;59(1):429–44. https://doi.org/10.1007/s12035-021-02607-3. Epub 2021 Oct 27. PMID: 34708329.
28. Shang JL, Ning SB, Chen YY, Chen TX, Zhang J. MDL-800, an allosteric activator of SIRT6, suppresses proliferation and enhances EGFR-TKIs therapy in non-small cell lung cancer. Acta Pharmacol Sin. 2021;42(1):120–31. https://doi.org/10.1038/s41401-020-0442-2. Epub 2020 Jun 15. PMID: 32541922; PMCID: PMC7921659.
29. Ribeiro M, Yordanova YN, Noblet V, Herbet G, Ricard D. White matter tracts and executive functions: a review of causal and correlation evidence. Brain. 2024;147(2):352–371. https://doi.org/10.1093/brain/awad308. PMID: 37703295.
30. Xie Y, Chen X, Li Y, Chen S, Liu S, Yu Z, et al. Transforming growth factor-β1 protects against LPC-induced cognitive deficit by attenuating pyroptosis of microglia via NF-κB/ERK1/2 pathways. J Neuroinflammation. 2022;19(1):194. https://doi.org/10.1186/s12974-022-02557-0. PMID: 35902863; PMCID: PMC9336072.
31. Ding L, Zhou J, Ye L, Sun Y, Jiang Z, Gan D, et al. PPAR-γ is critical for HDAC3-Mediated control of oligodendrocyte progenitor cell proliferation and differentiation after focal demyelination. Mol Neurobiol. 2020;57(11):4810–24. https://doi.org/10.1007/s12035-020-02060-8. Epub 2020 Aug 15. PMID: 32803489.
32. Zhou H, Liu S, Zhang N, Fang K, Zong J, An Y, et al. Downregulation of Sirt6 by CD38 promotes cell senescence and aging. Aging. 2022;14(23):9730–57. https://doi.org/10.18632/aging.204425. Epub 2022 Dec 6. PMID: 36490326; PMCID: PMC9792202.
33. Franklin RJM, Simons M. CNS remyelination and inflammation: from basic mechanisms to therapeutic opportunities. Neuron. 2022;110(21):3549–65.
34. Feldman JL, Baeza J, Denu JM. Activation of the protein deacetylase SIRT6 by long-chain fatty acids and widespread deacylation by mammalian sirtuins. J Biol Chem. 2013;288(43):31350–6.
35. Liszt G, Ford E, Kurtev M, Guarente L. Mouse Sir2 homolog SIRT6 is a nuclear ADP-ribosyltransferase. J Biol Chem. 2005;280(22):21313–20.
36. Molina-Gonzalez I, Holloway RK, Jiwaji Z, Dando O, Kent SA, Emelianova K, et al. Astrocyte-oligodendrocyte interaction regulates central nervous system regeneration. Nat Commun. 2023;14(1):3372.
37. Camargo N, Goudriaan A, van Deijk AF, Otte WM, Brouwers JF, Lodder H, et al. Oligodendroglial myelination requires astrocyte-derived lipids. PLoS Biol. 2017;15(5):e1002605.
38. Brambilla R. The contribution of astrocytes to the neuroinflammatory response in multiple sclerosis and experimental autoimmune encephalomyelitis. Acta Neuropathol. 2019;137(5):757–83.
39. Aharoni R, Eilam R, Arnon R. Astrocytes in multiple sclerosis-essential constituents with diverse multifaceted functions. Int J Mol Sci. 2021;22(11):5904.
40. Klotz L, Antel J, Kuhlmann T. Inflammation in multiple sclerosis: consequences for remyelination and disease progression. Nat Rev Neurol. 2023;19(5):305–20.
41. Theophanous S, Sargiannidou I, Kleopa KA. Glial Cells as Key Regulators in Neuroinflammatory Mechanisms Associated with Multiple Sclerosis. Int J Mol Sci. 2024;25(17):9588. https://doi.org/10.3390/ijms25179588. PMID: 39273535.
42. Holm RP, Wandall-Holm MF, Magyari M. Multiple sclerosis in Denmark (1950–2023): mean age, sex distribution, incidence and prevalence. Brain. 2024 Jul 20:awae245. https://doi.org/10.1093/brain/awae245. Epub ahead of print. PMID: 39031688.
43. Ryan L, Mills KHG. Sex differences regulate immune responses in experimental autoimmune encephalomyelitis and multiple sclerosis. Eur J Immunol. 2022;52(1):24–33. https://doi.org/10.1002/eji.202149589. Epub 2021 Nov 13. PMID: 34727577.
44. Tassoni A, Farkhondeh V, Itoh Y, Itoh N, Sofroniew MV, Voskuhl RR. The astrocyte transcriptome in EAE optic neuritis shows complement activation and reveals a sex difference in astrocytic C3 expression [J]. Sci Rep. 2019;9(1):10010.
45. Zhang AY, Elias E, Manners MT. Sex-dependent astrocyte reactivity: unveiling chronic stress-induced morphological changes across multiple brain regions [J]. Neurobiol Dis. 2024;200:106610.
46. Meadows SM, Palaguachi F, Jang MW, Licht-Murava A, Barnett D, Zimmer TS, et al. Hippocampal astrocytes induce sex-dimorphic effects on memory [J]. Cell Rep. 2024;43(6):114278.
47. Vergallo A, Lista S, Lemercier P, Chiesa PA, Zetterberg H, Blennow K, et al. Association of plasma YKL-40 with brain amyloid-β levels, memory performance, and sex in subjective memory complainers [J]. Neurobiol Aging. 2020;96:22–32.
48. Sanfilippo C, Castrogiovanni P, Imbesi R, Kazakowa M, Musumeci G, Blennow K, et al. Sex difference in CHI3L1 expression levels in human brain aging and in Alzheimer's disease [J]. Brain Res. 2019;1720:146305.
49. Kachanov A, Kostyusheva A, Brezgin S, Karandashov I, Ponomareva N, Tikhonov A et al. The menace of severe adverse events and deaths associated with viral gene therapy and its potential solution. Med Res Rev. 2024;44(5):2112–93.
50. Akter R, Afrose A, Rahman MR, Chowdhury R, Nirzhor SSR, Khan RI, et al. A comprehensive analysis into the therapeutic application of Natural products as SIRT6 modulators in Alzheimer's Disease, Aging, Cancer, inflammation, and diabetes. Int J Mol Sci. 2021;22(8):4180.
51. Jayachandran M, Wu Z, Ganesan K, Khalid S, Chung SM, Xu B. Isoquercetin upregulates antioxidant genes, suppresses inflammatory cytokines and regulates AMPK pathway in streptozotocin-induced diabetic rats. Chem Biol Interact. 2019;303:62–9.
52. Murakami A, Ohnishi K. Target molecules of food phytochemicals: food science bound for the next dimension. Food Funct. 2012;3(5):462–76.
53. Schröder LJ, Mulenge F, Pavlou A, Skripuletz T, Stangel M, Gudi V, et al. Dynamics of reactive astrocytes fosters tissue regeneration after cuprizone-induced demyelination. Glia. 2023;71(11):2573–90.
54. Chen T, Lennon VA, Liu YU, Bosco DB, Li Y, Yi MH, et al. Astrocyte-microglia interaction drives evolving neuromyelitis optica lesion. J Clin Invest. 2020;130(8):4025–38.
55. Wei Y, Chen T, Bosco DB, Xie M, Zheng J, Dheer A, et al. The complement C3-C3aR pathway mediates microglia-astrocyte interaction following status epilepticus. Glia. 2021;69(5):1155–69.
56. Xiao X, Hu H, Zhong Y, Chen Y, Tang K, Pan Z, et al. Microglia Sirt6 modulates the transcriptional activity of NRF2 to ameliorate high-fat diet-induced obesity [J]. Mol Med. 2023;29(1):108.
57. Song Y, Jiang W, Afridi SK, Wang T, Zhu F, Xu H, et al. Astrocyte-derived CHI3L1 signaling impairs neurogenesis and cognition in the demyelinated hippocampus. Cell Rep. 2024;43(5):114226.
58. Han Q, Xie QR, Li F, Cheng Y, Wu T, Zhang Y, et al. Targeted inhibition of SIRT6 via engineered exosomes impairs tumorigenesis and metastasis in prostate cancer. Theranostics. 2021;11(13):6526–41. https://doi.org/10.7150/thno.53886. PMID: 33995674; PMCID: PMC8120217.

59. Wang S, Sdrulla AD, diSibio G, Bush G, Nofziger D, Hicks C, et al. Notch receptor activation inhibits oligodendrocyte differentiation. Neuron. 1998;21(1):63–75.
60. Zhao T, Su Z, Li Y, Zhang X, You Q. Chitinase-3 like-protein-1 function and its role in diseases. Signal Transduct Target Ther. 2020;5(1):201.
61. Zou Y, Zhang J, Xu J, Fu L, Xu Y, Wang X, et al. SIRT6 inhibition delays peripheral nerve recovery by suppressing migration, phagocytosis and M2-polarization of macrophages. Cell Biosci. 2021;11(1):210.
62. Zou Y, Zhang J, Liu J, Xu J, Fu L, Ma X, et al. SIRT6 negatively regulates Schwann cells dedifferentiation via targeting c-Jun during Wallerian Degeneration after Peripheral nerve Injury. Mol Neurobiol. 2022;59(1):429–44.
63. Ding L, Zhou J, Ye L, Sun Y, Jiang Z, Gan D, et al. PPAR-γ is critical for HDAC3-Mediated control of oligodendrocyte progenitor cell proliferation and differentiation after focal demyelination. Mol Neurobiol. 2020;57(11):4810–24.
64. Chu T, Zhang YP, Tian Z, Ye C, Zhu M, Shields LBE, et al. Dynamic response of microglia/macrophage polarization following demyelination in mice. J Neuroinflammation. 2019;16(1):188.
65. Favrais G, Saliba E, Savary L, Bodard S, Gulhan Z, Gressens P, et al. Partial protective effects of melatonin on developing brain in a rat model of chorioamnionitis. Sci Rep. 2021;11(1):22167.
66. Huang P, Zhou Q, Lin Q, Lin L, Wang H, Chen X, et al. Complement C3a induces axonal hypomyelination in the periventricular white matter through activation of WNT/β-catenin signal pathway in septic neonatal rats experimentally induced by lipopolysaccharide. Brain Pathol. 2020;30(3):495–514.

Publisher's note